NASA CONTRACTOR
REPORT

NASA CR-170668

BREAD BOARD FLOAT ZONE EXPERIMENT SYSTEM FOR HIGH PURITY SILICON

By Westech Systems, Inc.
3502 E. Atlanta Avenue
Phoenix, Arizona 85040

June 17, 1982

Final Report

Prepared for

NASA-George C. Marshall Space Flight Center
Marshall Space Flight Center, Alabama 35812

TECHNICAL REPORT STANDARD TITLE PAGE

1. REPORT NO.	2. GOVERNMENT ACCESSION NO.	3. RECIPIENT'S CATALOG NO.
NASA CR-170668		

4. TITLE AND SUBTITLE	5. REPORT DATE
Bread Board Float Zone Experiment System for High Purity Silicon	June 17, 1982
	6. PERFORMING ORGANIZATION CODE JA64
7. AUTHOR(S) Edward L. Kern/Gerald L. Gill, Jr.	8. PERFORMING ORGANIZATION REPORT #
9. PERFORMING ORGANIZATION NAME AND ADDRESS Westech Systems, Inc. 3502 E. Atlanta Avenue Phoenix, Arizona 85040	10. WORK UNIT NO. RTOP 179-70-62 11. CONTRACT OR GRANT NO. NAS8-34542
12. SPONSORING AGENCY NAME AND ADDRESS National Aeronautics and Space Administration Washington, DC 20546	13. TYPE OF REPORT & PERIOD COVERED Contractor Report 14. SPONSORING AGENCY CODE

15. SUPPLEMENTARY NOTES

Technical Manager: I. C. Yates, Marshall Space Flight Center, AL.

Final Report

16. ABSTRACT

A float zone breadboard system based on a commercial float zone system has been placed into operation to support theoretical and experimental investigations on the float zone process. The objective of these investigations is to more fully understand the limitations of the process on Earth, particularly with regard to the role of gravity in flows in the molten zone. The breadboard will also be used to evaluate concepts for improving the process in one-g and for conducting experiments in microgravity.

17. KEY WORDS	18. DISTRIBUTION STATEMENT
Float Zone; Single Crystal Growth; Materials Processing in Space	Unclassified-Unlimited Harvey Herring

19. SECURITY CLASSIF. (of this report)	20. SECURITY CLASSIF. (of this page)	21. NO. OF PAGES	22. PRICE
Unclassified	Unclassified	57	NTIS

MSFC - Form 3292 (May 1969)

For sale by National Technical Information Service, Springfield, Virginia 22151

TABLE OF CONTENTS

	PAGE
Introduction and Summary	1
I NASA Breadboard Zoner	3
A. Acquisition	3
B. Installation	6
C. Operation	7
D. Required Future Modifications	7
II Characterizing the Molten Zone	10
A. Growth of Crystals	10
B. Methods of Characterization	10
C. Striation Etching	15
D. Effect of Growth Conditions on Melt Characteristics	19
III Improved Coil Studies	33
A. Shorted Ring Coil	33
B. R.F. Coil Slice Heating	39
C. Proposed Studies	42
IV Concepts for Precursory Flight Experiments	46
A. Silicon Slice Experiments	46
B. Thin Rod Zoning	48
C. Si : Ge Crystals	53
D. Flight Possibilities	53
List of References	55

INTRODUCTION AND SUMMARY

This is the final report on Contract NAS 8 - 34542 "Breadboard Float Zone Experiment System for High Purity Silicon", with a seven month contract period from 17 November, 1981 to 17 June, 1982. This contract was performed for NASA's George C. Marshall Space Flight Center, and was monitored by Mr. I.C. Yates.

A breadboard float zone experimental system has been established at Westech Systems for use by NASA in the float-zone experimental area. A used zoner of suitable size and flexibility was acquired and installed with the necessary utilities. Repairs, alignments and modifications were made to provide for dislocation-free zoning of silicon. The zoner is capable of studying process parameters used in growing silicon in gravity and is flexible to allow trying of new features that will test concepts of zoning in microgravity. Growth of one-inch diameter crystals was demonstrated to the Float Zone Working Group on February 23, 1982.

Characterizing the state-of-the-art molten zones of a growing silicon crystal will establish the data base against which improvements of zoning in gravity or growing in microgravity can be compared. 25 mm diameter was chosen as the reference size, since growth in microgravity will be at that diameter or smaller for about the next 6 years. Dislocation-free crystals were grown in the <100> and <111> orientations, using a wide set of growth conditions. The zone shape at one set of conditions was measured, by simultaneously aluminum doping and freezing the zone, lengthwise slabbing and delineating by etching. The whole set of crystals, grown under various conditions, were slabbed, polished and striation etched, revealing the growth interface shape and the periodic and aperiodic natures of the striations. This data will be analyzed to study melt dynamic considerations. Zone shape data is being supplied to M.I.T. for consideration in their float-zone model. Initial analysis is included in the report, with more detailed analysis being planned for a future experimental program.

New coil designs are desired which will minimize or eliminate the effects of the present coil slot. The slot causes a minimum in the heating r.f. field which gives rise to microscopic inhomogeneities in resistivity, other impurities and crystal defects. These, in turn, effect the behavior of critical silicon devices. Coils made with a slotted coil transforming to an inner shorted ring provided the coupling of power into the shorted ring, but it, in turn, did not couple power to a work load (graphite or silicon). The need for analytically studying r.f. coil fields is apparent. Design concepts to improve the slotted coils field have been developed.

Growth of silicon crystals in microgravity at diameters useful in semiconductor device lines (25 to 100 mm diameter) will take development time and more power than is available on the shuttle for several years. Can we determine the advantages of microgravity and characterize key growth phenomena by experiments which can be carried out in the interim? Study of the available experimental arrangements, various phenomena to be characterized and low power experimental equipment indicate this is feasible. Growth of silicon fromtthe melt in the shape of a silicon slice should provide experimental characterization of the Marangoni flow. Ground-based experimental equipment is being assembled at Marshall Space Flight Center to test this concept. Zoning of small diameter (5 mm) rods should be possible by modifying the ADSF (Advanced Directional Solidification Furnace) used on Spar sounding rockets. This would help in characterizing the use of alternative heating methods (hot wall), the behavior of gas (without convection) as a zoning atmosphere, and the role of Marangoni flow in a rod form (low to medium aspect ratio). Both experimental configurations would be suitable to growth of both silicon and silicon-germanium alloys. Ground-based investigations could be completed within a year, with flights possible in the 1984-86 period.

I. NASA BREADBOARD ZONER

The purpose of this effort was to establish a state-of-the-art float zoning capability for silicon that will be used in the NASA Float Zone Working Group scientific program. Its' use is available to all investigators on NASA programs. It is expected that investigators will suggest process changes, or may wish to participate in process studies or analysis using the zoner.

A. Acquisition

Selection of the particular Float Zone Refiner (FZR) unit was made on the basis of several criteria. The FZR was originally manufactured by Westech Systems, Inc. (WSI), thus modification and maintenance capability will be enhanced by familiarity with the machine construction. This particular Zoner is quite versatile; it is capable of high vacuum or gas zoning and can also be utilized for gas doping. The main chamber is equipped with 2 user ports; one is 19 cm diameter, the other is 6.4 cm. These ports are in addition to the door viewing port and are positioned to allow access to the zone area by video, infrared or other scanning or monitoring equipment.

Figures 1 & 2 depict the zoner and an internal view of the main chamber, respectively. The following table is a summary of the performance specifications.

1. Material Size

Maximum feed rod travel length	61 cm.
Maximum finished crystal travel length	61 cm.

2. Zoning Environment

Gas	Argon, Helium, etc.
Vacuum	Diffusion Pumped High Vacuum System (10^{-6} torr)
Gas Doping	Gas plus diluent. Control unit must be added.

3. Growth rates (both transports)

Slow	0 - 75 mm/min.
Fast (for rapid transport positioning only)	2000 mm/min.

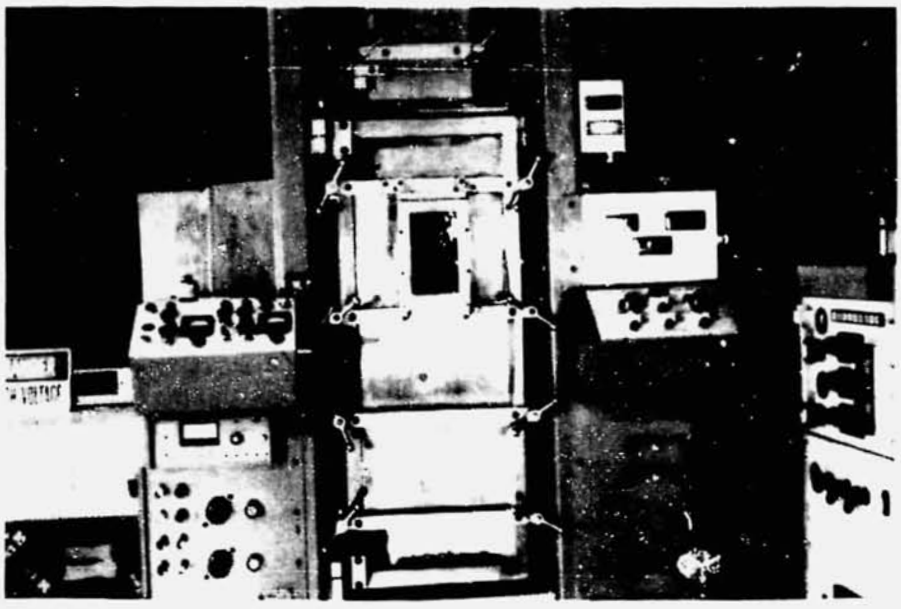

Figure 1 - NASA Breadboard Zoner, Showing (from left) the r.f. and vacuum controls, zoning chamber, speed control and gas control panel

Figure 2 - Inside of Zoning Chamber. The r.f. coil is on the left, with a silicon polycrystal feedrod above it and graphite preheater below. At the bottom is the silicon seed in its chuck.

Figure 3 - Installed NASA Breadboard Zoner. The r.f. generator is at the left, the deionized cooling water for r.f. circuits at right. Power and water lines are attached to the back wall.

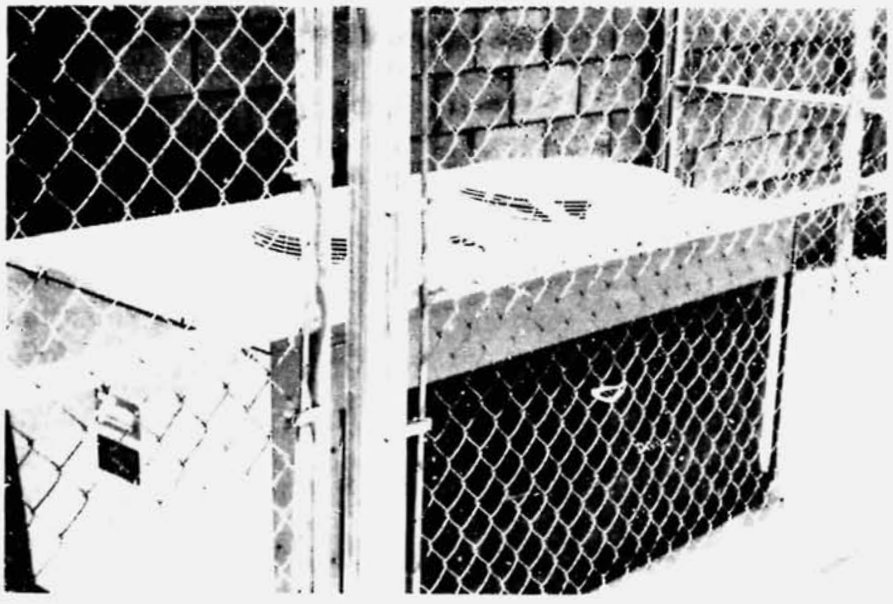

Figure 4 - External water chiller for regulating cooling water temperature.

4. R.F. Power Supply

Power Input	80 KW max.
Power Output	50 KW max.
Frequency	2.7 mhz

B. Installation

The installation of the zoner involved three phases:

1. Preparation of the facility.

2. Assembly and interconnection of the zoner with the requisite plant services.

3. Maintenance and required modifications to allow performance of the preliminary experiments.

The zoner system requires a large quantity of deionized, temperature stabilized cooling water. A source of clean air is required. Electrical power must be adequate for the R.F. Power Supply. All of these services were installed either prior to or just after the zoner was delivered. Figure 3 shows the zoner installation, including the deionized cooling water reservoir at the right. The water chilling unit was installed on a specially prepared pad outside the building. (See Figure 4) A 950 liter reservoir with appropriate pumps was installed adjacent to the zoner. Electrical power disconnects and switching units for the water pumps and chiller were installed at appropriate locations. Electrical power and cooling water connections were made to the zoner and the R.F. Power Supply. Plumbing and connection of the roughing vacuum lines and the roughing vacuum pump completed the first two phases of the installation.

The machine had been out of service for some time prior to delivery to Westech. For this reason, it was necessary to perform a thorough maintenance procedure. This included disassembly and cleaning of the chamber seals and the transport drive mechanisms. Defective and worn parts were replaced. The transport motion control systems were recalibrated to millimeters per minute. The transports were adjusted to ensure that the work shafts were axially centered and vertically aligned. Some machine work was required on the r.f. zoning coil mount block to ensure centering the coil with respect to the work shafts. A defective Power Tube was found in the R.F. Power Supply; this was replaced and appropriate calibration and frequency adjustments were made.

The gas system required several modifications. The gas valves were not vacuum tight and were subject to vacuum lock-out on backfilling the chamber with argon; these were replaced. The vacuum vent valve was of insufficient size to allow rapid backfilling of the chamber to bring up to atmospheric pressure, so this valve was replaced also. The Westech Standard Gas System (commercially supplied on zoners) was installed to provide faster, more accurate and reliable gas control.

The vacuum system was tested for leaks and these were corrected.

C. Operation

The purpose of the zoner is to grow silicon crystals under very exact growth conditions. Initial operation indicated better physical alignment of the shafts and r.f. coil were required. Initial zoning produced single crystals. Figure 5 shows a crystal being zoned inside the zoner. Dislocation-free crystals were first zoned in February, and the zoner was growing crystal at the time of the Float Zone Working Group visit on February 23, 1982

Growth of crystals under a wide variety of conditions was accomplished with the aid of consultant Ronald Schultz of Sanford, Michigan, who donated his time to this program. The set of crystals grown under these varying conditions are shown in Figure 6 . The crystal on the right was increased to 37 mm (1.5 inch) diameter. The second from the right was the crystal where the melt was decorated with aluminum. All other crystals are 25 mm dislocation free; the far left crystal is <100> orientation, with the remainder being < 111> .

The zoner has proven it can repeatedly zone dislocation free crystals to the lengths necessary for these studies, including growth at high speeds (5 mm/min. and 30 rpm) and low speeds (1 mm/min. and 6 rpm) without generator or transport problems.

D. Required Future Modifications

The zoner, as purchased, was designed to operate in a production environment. Several of the control system components do not provide the high accuracy necessary for precise characterization of state of-the-art silicon zoning and development leading to microgravity experiments. In particular, the controls for growth rate and the motors do not provide the velocity control accuracy nor the velocity range capability required, especially for very slow speed zoning. The R.F. Power Supply exhibits some instability at light loading and it does not provide sufficient power regulation. There are no interface mechanisms to allow recording of growth parameters or computer monitoring or control. The following schedule delineates the modifications necessary to prepare the zoner for the exacting research work required of it.

1. Install the Westech (commercial zoner design) phase locked translation Motor Control System. This includes low inertia motors and integral, precision gearboxes and optical digital encoders.

2. Replace the R.F. Power Supply control circuitry with the Westech Dropper Tube Power Control Regulator System. This would include the Dropper Tube filament transformer & the associated closed loop control component modules.

3. Install Data Acquisition Modules that will allow computer access of Translation Velocity, Rotation Rate and RF Power Set Point.

Figure 5 - Growth of a Silicon crystal. The seed is at the bottom, with the tapered transition above it. The melt begins where the material starts decreasing in diameter.

Figure 6 - Crystals grown in the NASA Breadboard Zoner. (These are mounted on graphite, ready for sawing)

II. CHARACTERIZING THE MOLTEN ZONE

Growth of silicon crystals by float zoning provides crystals of superior purity, which are used to make many critical devices that control electrical power and detect light, infrared heat and x-rays. The growth technique involves a high degree of operator skill. Considerable improvements have been made in growth processes by studying and changing process parameters. However, the solid-melt growth system has not been studied analytically and melt properties and phenomena are not well characterized. Predicting the advantages of processing in microgravity will require seperating gravity influenced phenomena (such as bouyancy convection) from phenomena not affected by gravity(such as surface tension driven convection). Models are being developed using numerical computor techniques (at M.I.T.). The effects of these phenomena must be determined experimentally, under controlled growth conditions, to correlate to the models. This will begin by characterizing crystals grown under known conditions by present state-of-the-art techniques.

A. Growth of Crystals

Crystals have been grown at one inch diameter in the NASA Breadboard Zoner. Initial growth attempts, while the equipment was being tested and growth skills developed, resulted in several crystals which were not dislocation-free. Dislocation free growth techniques were acquired from Mr. Ronald Schultz of Sanford, Michigan, who both grew crystals and taught the Westech operator. Figure 6 shows the dislocation-free crystals grown. Table 1 lists the crystals and the growth conditions under which they were grown.

B. Methods of Crystal Characterization

The molten zone and grown crystal need to be characterized to provide the experimental counterpart to the computor model of growing. This involves the shape of the molten zone and freezing interface. The exterior shape can be captured photographically during growth, with the coil obscuration being eliminated by splitting the image by photographing at an angle below the melt and another above the melt.

A technique was developed by Keller[1] to show both exterior surfaces and the molten-solid interfaces by injecting aluminum into the melt (see Figure 7) and rapidly solidifying, with the top and bottom rods included in the frozen structure. This is then sawn lengthwise and etched (using a modified CP4 etch of nitric, acetic & hydroflouric acids) to show the former melt shape. Figure 8 shows the crystal grown (on left), the doped melt with the frozen expansion tip protruding toward the bottom of the picture, and the poly feed rod (right). The etched cross-section slab is shown in Figures 9 and 10 . Figure 9 shows the seed and crystal portion on the left, the brightly colored aluminum-alloy showing where the melt was and the ingot being melted to the right of the melt.

Table 1 Silicon Crystals Grown for Characterization Program

Crystal No.	Orient.	Total Length cm.	Crystal Growth Speed (mm/min)	Lower Rod Rotation Rate rpm	Upper Rod Rotation Rate rpm
82-03-000	<100>	10	2.9	14.5 c.w.	1.2
82-03-001a	<100>	7	2.7	5.2	0
82-03-001b	<100>	20	2.8	6.0	0
82-03-002	<111>	20	4.1	14.6	1
82-03-003	<111>	25	4.0	15	0
			4.0	15	.7 c.c.w.
			3.0	0	.7
			4.0	15	.7
			2.0	15	.7
			2.0	15	-.7 c.w.
82-03-004	<111>	23	2.1	15	0
			2.1	6	0
			2.1	22	0
			2.1	30	0
			5	30	0
82-03-005	<111>	20	5	15.6	0
			4	15.6	0
			2	15.6	0
			1	15.7	0
82-03-006	<111>	3	2.8	10.2	1
	Melt Aluminum doped and quenched				
82-03-007	<111>	17	2.9 (2.5 cmD.)	15.5	0
			1.9 (3.7 cmD.)	15.5	0
	Coil has modified slot				

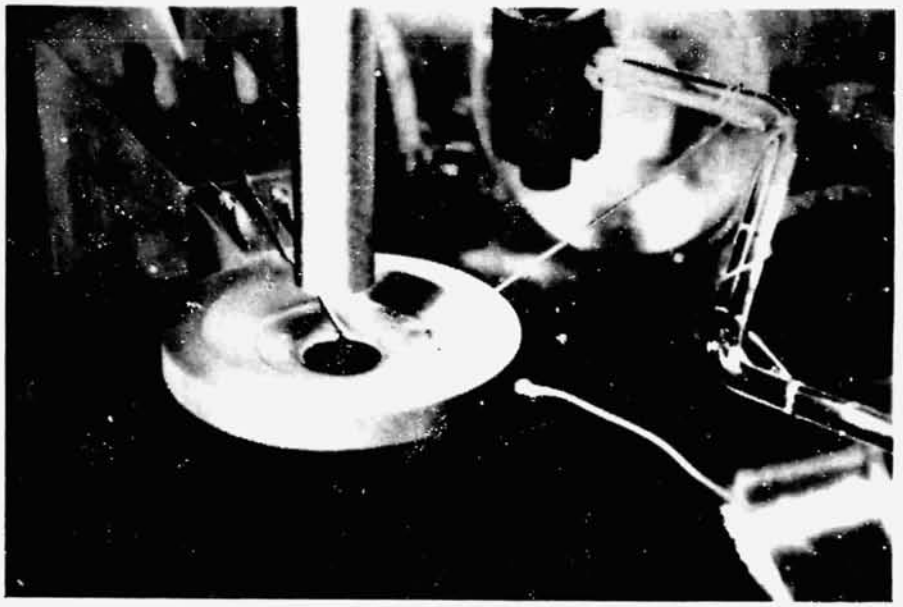

Figure 7 Aluminum doping setup, showing high purity aluminum wire on the preheater arm, which can be injected into the melt from above the coil.

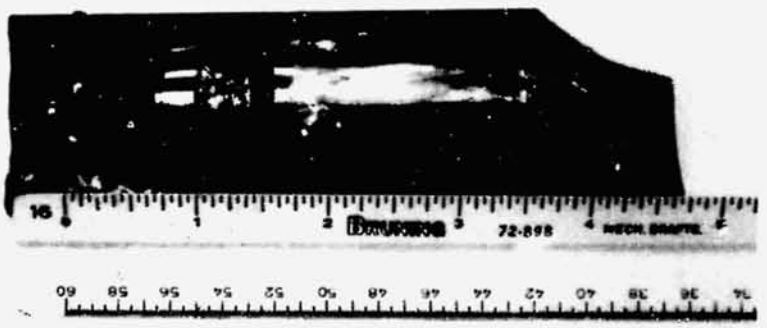

Figure 8 Aluminum - doped melt crystal.

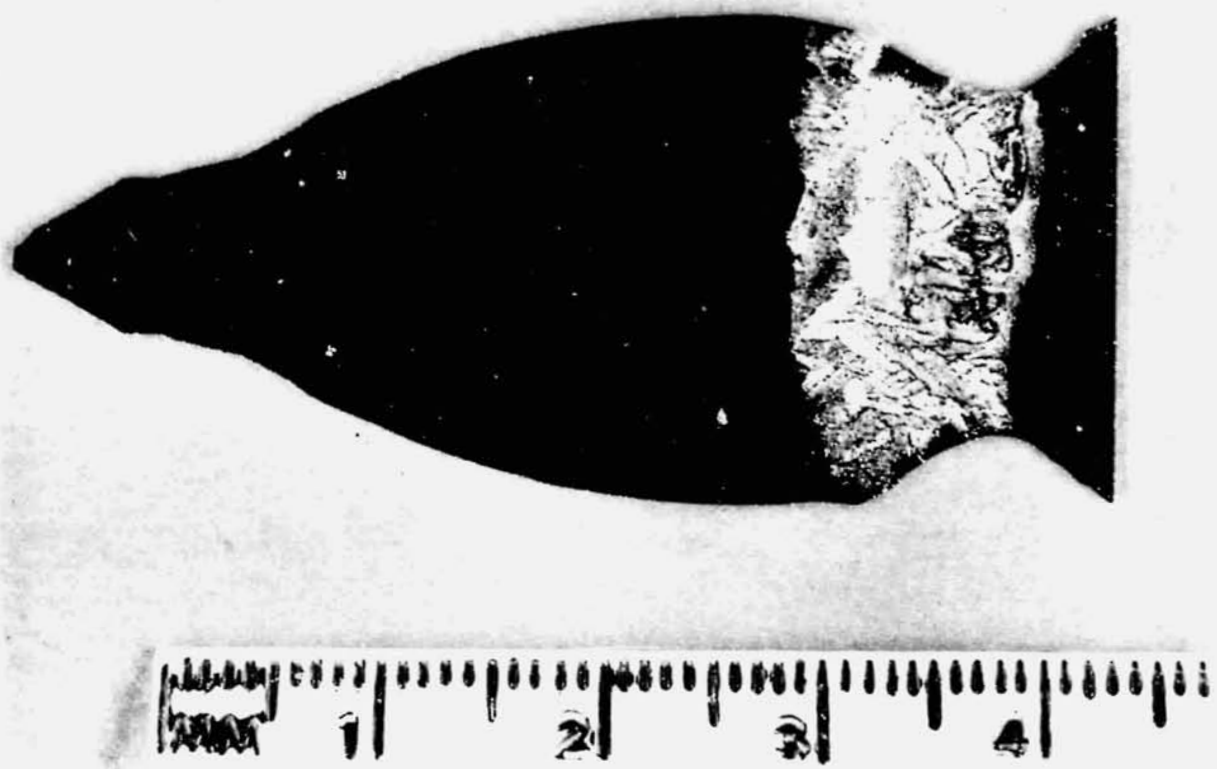

Figure 9 - Aluminum decorated silicon melt.

Figure 10 - Close up of aluminum decorated melt of Figure 9 .

Figure 10 is a close-up view of the same melt.

The growth interface shape can also be seen in resistivity striations which can be etch-decorated. The hot spot in the coil (close to the slot) gives rise to a rapid melting of previously grown crystal, followed by a rapid freezing. This gives rise to an increase in impurity concentration due to the higher effective segregation coefficient at higher instantaneous growth speeds. This leads to a microscopic suddenly lower resistivity (striation), which is preferrentially etched by etchants which are specific for higher chemical activity. This procedure and the results are described in section C below. From previous studies, it is also known that non-doping impurities, such as carbon, and crystal defects (swirls) are also concentrated at the striation lines. This sudden change in growth speed does indicate the shape of the melt-crystal interface at that point in time.

C. Striation Etching

Obtaining etched striation patterns that are easy to analyze in the microscope and to photograph requires good sample preparation. Figure 11 shows the I.D. diamond blade saw used to obtain the slabs for analysis, which were usually cut lengthwise down the center of the cylindrical crystal. The slabs are then hand lapped with 12 μm SiC powder in water on glass plates to remove saw marks and other surface irregularities. They are then chemically polished in a modified CP4 (5 parts HNO_3, 3 parts acetic acid, 2 parts HF). This surface can be directly striation etched, but the appearance under the microscope is not as good as for chemical-mechanically polished surfaces. The latter is done on the Westech double-sided polisher shown in Figure 12 . One side is polished, using the top plate for pressure and using a special cutout in the mylar sheet which holds the slab. In this manner, non-round slabs can be polished.

The striation etching procedure is described in Table 2 . This is a modification of the Mayer and Kamperer etches.[3] Figure 13 shows the etching hood with I.R. lamp, variac and timer.

Since the striation etch was originally developed for more heavily doped crystals (1 ohm-cm Si : Ga), changes had to be made to bring out the striation lines more distinctly in this undoped (except for residual poly impurities) silicon of high resistivity (one crystal was 1500 ohm-cm p-type). Longer etching times (20 minutes), under slightly more intense light (80% variac setting), more acetic acid buffering (300 ml.) and more wetting agent (20 drops) was found to be the best.

These striation etching conditions are so long that oxidation of the surface either introduces spots to obscure some of the etched lines or a total dense covering of oxide. We have reached the limit of this etching technique. It is recommended that a light doping of gallium be used to make the demarcation etching easier. Professor Brown (M.I.T.) has requested doping to show radial gradients to show the effect of flow, and gallium would be an ideal dopant. A good dopant to show fast transient effects would be phosphorus,

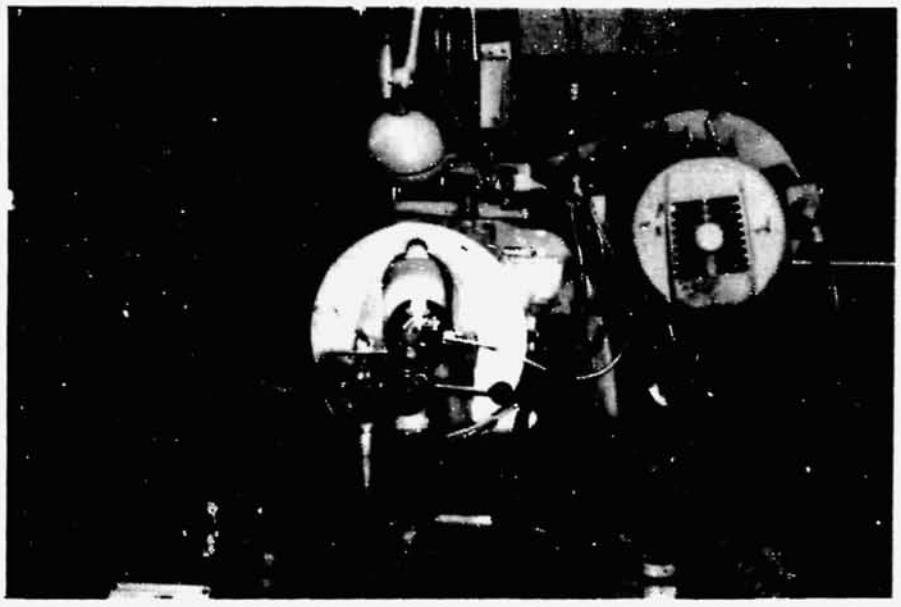

Figure 11 Diamond-blade saw for slicing and slabbing silicon crystals.

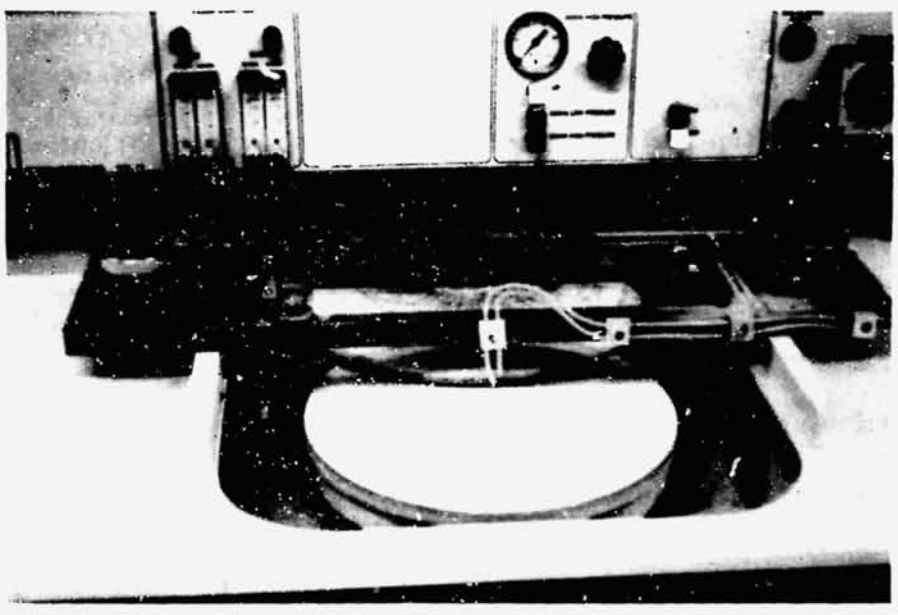

Figure 12 Double-sided polisher for chemical-mechanically polishing silicon slabs. Note mylar sheet carrier to hold slices between the upper and lower, rotating, plates.

Table 2 - Striation Etching Procedure

Step 1	Lap, chemically polish with CP4 and chemical/mechanical polish
2	CP4 polish with 5 cm^3/cm^2 surface area Stop with equal amount of HNO_3 Dilute with D.I. water
3	Transfer to Acetic Acid without the surface drying
4	Transfer to fresh etching solution without the surface drying: 200 ml HF 300 ml Acetic Acid 20 drops wetting agent (Photo-Flo 200) 2.0 gm $NaNo_2$ Illuminate with 250 watt I.R. bulb (Variac at 80%) Duration: 20 minutes
5	Rinse in D.I. water and methanol and blow dry

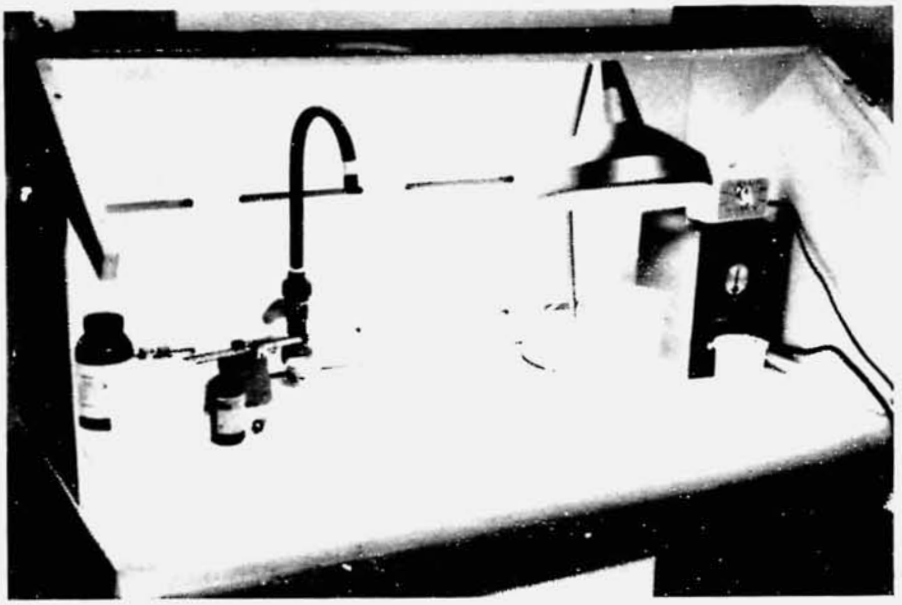

Figure 13 - Etching hood and sink. The I.R. lamp, variac (variable transformer) and timer used for striation etching are at the right.

with a relatively high segregation coefficient (approximately 0.6).

The striations can then be observed in a bright field microscope with Nomarski (phase interference contrast) objectives. This is an Olympus model BH unit, with halogen lamp, magnifications from 50 to 1000 and an automated exposure Polaroid-back camera. (see Figure 14).

A slab, which has been polished and striation etched, is shown in Figure 15. This slab shows the seed at right, for a <111> crystal.

D. Effect of Growth Conditions on Melt Characteristics

The crystals were striation etched and analyzed by the Nomarski microscope to reveal some of the characteristics of the melt-freezing interface system. The delineation of striations was light and often obscured by oxide films and not all of the growth parameters could be followed. The growth conditions will be repeated, in large part, using Ga doping on the follow-on effort. Characteristics of the grown crystal are divided into the several catagories of information, as striation etching reveals the results from the freezing interface:

1. Growth Interface Shape. The curvature of the growth interface, as delineated by the major stria (rotational meltback striations), changes as the diameter changes. The curvature can be characterized as:

from seed (3 mm diameter) to 14 mm diameter	convex (toward melt)
at 14 mm	flat
> 14 mm	concave
at 15 mm (decreasing to close crystal off at tang end)	flat to slightly convex
15 mm (at top of tang end)	concave

Figure 16 shows the convex nature of the striation at the seed end of a <100> crystal (000 slab 1). The faceted interface of a <111> crystal at full diameter (crystal 003 slab 1) is shown in Figure 17. This composite photograph was made by photographing the interface at 50 x in 23 horizontal steps. The vertical scale is the same as the horizontal, with each minor division being 22.2 μm. The interface shape can be taken from this figure for correlating to models under these same growth conditions of:

orientation : <111>

diameter : 25 mm

average growth rate: 3.4 mm/min

ORIGINAL PAGE
BLACK AND WHITE PHOTOGRAPH

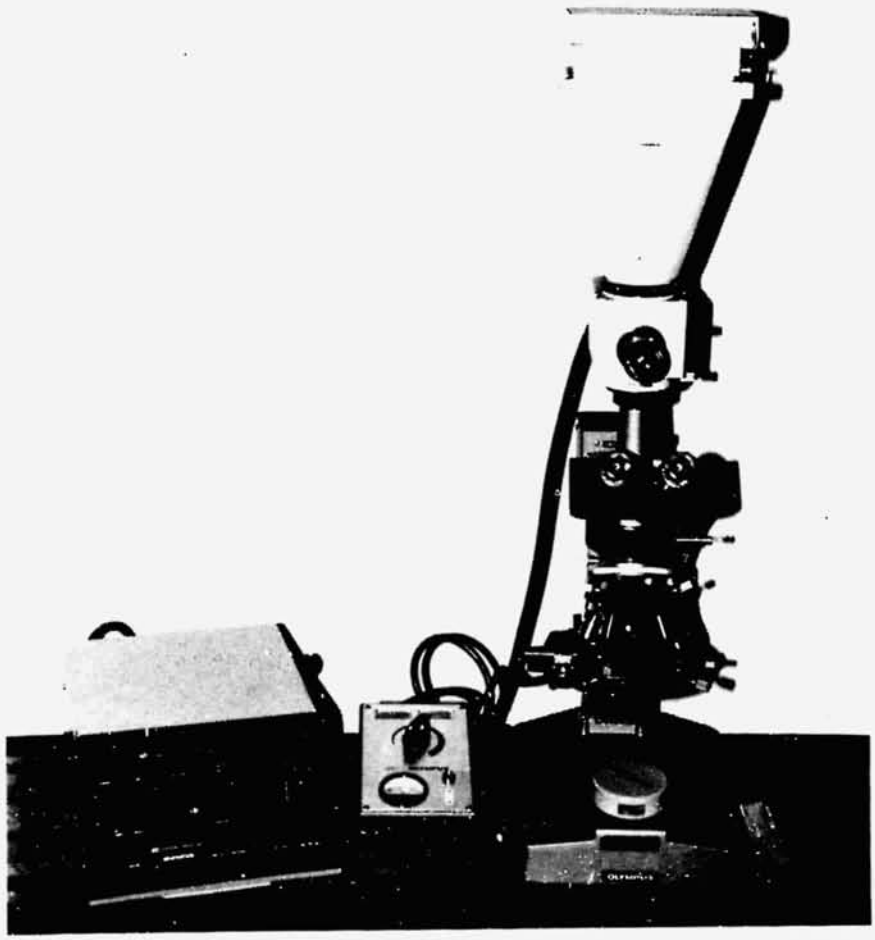

Figure 14 - Olympus Nomarski microscope with Polaroid camera for striation photography.

Figure 15 - Polished and Striation Etched Slab. <111> crystal 007 slab 1; seed is at the right.

Figure 16 - Convex striation at seed end of <100> crystal. Crystal 000 slab 1. Note curved line under scale. Melt is at the top; grown at the bottom

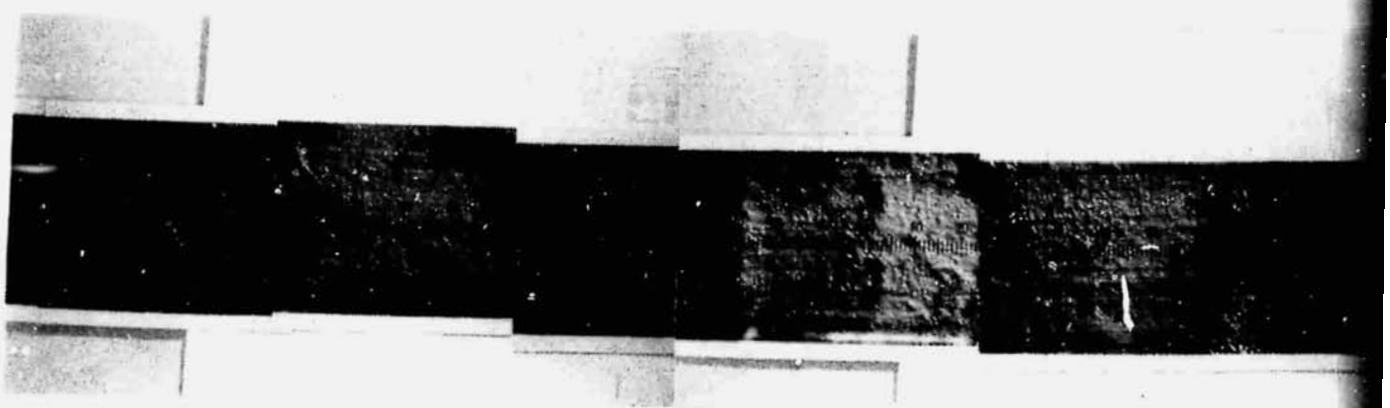

Figure 17 - Growth Interface Shape of <111> dislocation free crystal. Composite microphotograph on striation etched slab.

FOLDOUT FRAME

Lower rotation rate : 15 rpm
(of crystal)

Upper rotation rate : 0
(of feed rod)

2. Concavity of major striations. The concavity (distance in the axial direction between the highest and lowest points of the growth interface) varies markedly between <100> and <111> crystals. A <100> crystal (000 slab 1 grown at 3 mm/min. at 14.5 rpm lower and 1.2 rpm upper at 27 mm diameter) has a simple concave shape, with the center being 3.7 mm lower than the edge. <111>crystals have a central facet which is higher than the curved interface toward the edges of the crystal. Table 3 indicates the degree of concavity under various growth conditions. From the <111> crystal interface shape, it can be assumed that the isotherms near the growth interface are a W-shape : high at the outsides and center and with a minimum at roughly 2/3 of the radius. If this is correct, then the center of a very concave <100> growth interface is very undercooled and should incorporate impurities at higher concentrations than at the edges of the crystal. As seen on crystal 004, the curvature of the growth interface shape changes markedly with growth rate and probably indicates a marked difference in bouyancy convection velocities.

3. Spacing and shape of major striations. The variation in zoning speeds can be determined from the variation of distances between the major striations caused by the growing interface reacting with the cold spot of the r.f. coil. This produces a helical front with a spacing determined by the rotation and translation rates of the growing crystal. While we cannot yet measure the instantaneous speeds of either accurately (which will be done in the follow-on program), it will be assumed that the rotation rate is constant. This is a reasonable assumption since the mechanical drive train is very simple compared to the drive train for translation. Crystal 004 (slab position 5) shows speeds of:

5.13 mm/min.

5.82 mm/min.

5.13 mm/min.

4.96 mm/min.

over a 4 second period, or a 16% maximum variation, based on the average velocity. The lines also were bending, with the interval between any two lines being variable, as shown in Figure 18. At a slower speed of 2.1mm/min. on the same crystal, the variation was 22%. Crystal 004 (position 5) showed a 12% variation at 5.33 mm/min.

Table 3 - Growth Interface Concavity

Crystal	Orientation	Growth Rate mm/min.	Upper Rotation rpm	Lower Rotation rpm	Concavity (mm)	
					Edge to min.	minimum to center for 111
000 slab 1	<100>	3	14.5	1.2	3.7	-
003 slab 1	<111>	3.4	15	0	.28	
004 slab 5	<111>	2.05	30	0	1.1	.33
004 slab 5	<111>	5.26	30	0	.44	.66

Figure 18 Major striations in crystal 004 (position 5) showing variation between lines and bending of lines (50 x)

Figure 19 Intersection of <111> growth flat (right) and curved interface (left) for <111> crystal 003. Note feathering (minor striation) at the intersection (50 x, each division= 22.2 μm).

The intersection of the <111> growth plateau in the center of the crystal and the curved interface is shown in Figure 19 for crystal 003 (slab 1) at an average growth rate of 3.37 mm/min. Figure 20 shows a different part of the same slab, with an average growth rate of 4.08 mm/min. The curved feathers are similar to the F_{21} feathers of Bauser and Rozgonyi[4], which they describe as an interaction between type I (striations delineating the instantaneous position of the solid-liquid interface or major striations) with type II (the instantaneous positions of laterally advancing terraces) striations.

The growth interface changes angle when the crystal changes diameter. Figure 21 shows the shift from decreasing diameter (division 30, where lines are perpendicular to the overall growth direction of the crystal) to increasing diameter (division 70)near the crystal center. This is a <100> crystal (000 slab 1) and the striations do not lie on a given crystallographic plane. Figure 22 shows the bending at the surface of the crystal. In the left photo, the diameter is decreasing and the lines are bending toward being parallel to the surface (stria at division 62). The right photo has the lines bent in the opposite direction, also tending toward being parallel to the surface.

4. Swirl. Both type A and B swirls are observed in these dislocation-free crystals. These are defined in reference 1 p. 193. The large A-swirl are caused by collapsing B-swirl. Figure 23 shows two A-swirl, with the triangular one at division 30 having sides of 59,28 and 59 μm length. The linear A-swirl at division 68 is 36 μm long. The B-swirl are about 3 to 6 μm diameter hillocks (see division 33 and 35). This was at a growth rate of 4.95 mm/min,, which deKock[5] claims is fast enough to avoid swirl. Figure 24 shows similar A and B-swirl types on the same crystal. Figure 25 shows that these are not clustered at the striations. These are for a <111> crystal.

For the <100> crystals, with more concavity, the B-swirls precipitate primarily on the major striations, with a few on the minor striations. Figure 26 shows this for crystal 001 slab position 2 (3 mm/min. growth rate at 6 rpm). Major striations are at divisions 35 and 65. Close viewing shows that the B-swirls are formed in the region grown immediately after the growth striation. On circular slices cut perpendicular to the growth direction, the striations are concentric circles, with the swirl concentrated on them.

Very few swirl are seen when the growth interface is convex or flat. It appears that a concave interface leads to swirl and that the very deep concaves of <100> crystals lead to many B-swirl precipitated on striations. When this precipitation does not occur (as for <111> crystals) the B-swirl are free to migrate and collapse to form A-swirl.

5. Minor striations. Minor, feathering-type, striations always occur between the major striations. These can be seen in Figures 20, 21, 22, and 26. Based on the instantaneous growth rates determined by the major striations, their periodicity in distance and time can be determined. Table 4 shows this

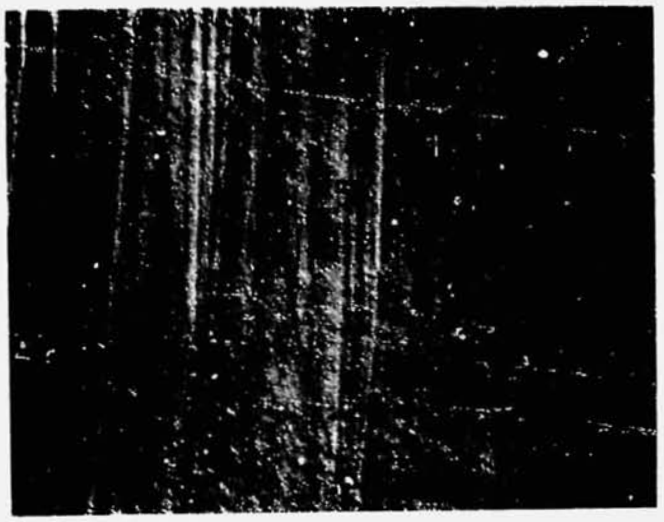

Figure 20 Intersection of <111> plateau (top) with curved growth interface, showing the large curved feather. Crystal 003 slab 1 (50 x, each division = 22.2 μm).

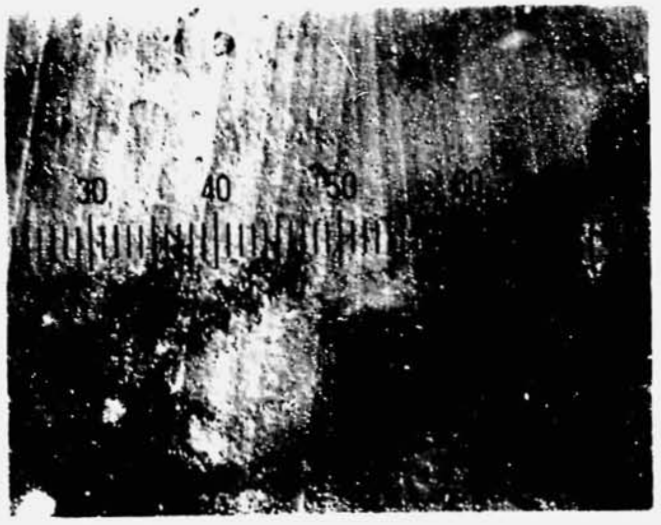

Figure 21 Change of striation direction going from decreasing diameter (division 30) to increasing diameter (division 70) (50 x, each division = 22.2 μm).

Figure 22 Striations at the surface of a decreasing (left) and increasing (right) diameter. The regions are adjacent to each other. (50 x, each division = 22.2 μm).

Figure 23 A and B-swirl (crystal 004 slab 5 <111>) (400 x, each division = 2.8 μm).

Figure 24 A and B-swirl (also on crystal 004 slab 5) (200 x, each division = 5.6 μm).

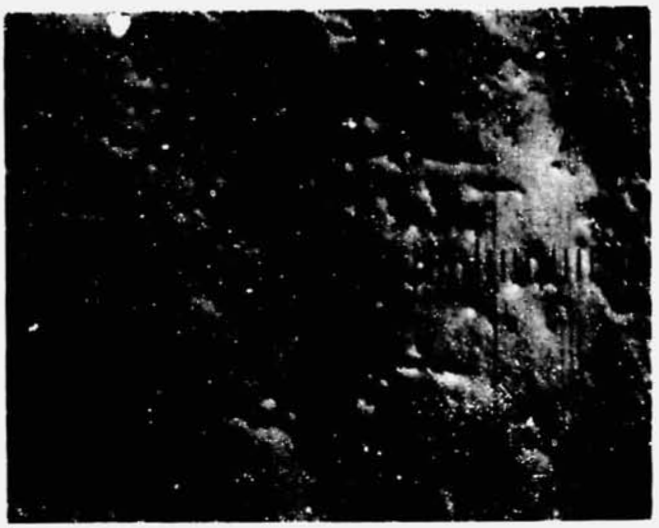

Figure 25 A and B-swirl and striations of crystal 004 slab 5 (< 111>) (50 x, each division = 22.2 μm) (average growth rate = 5.3 mm/min.).

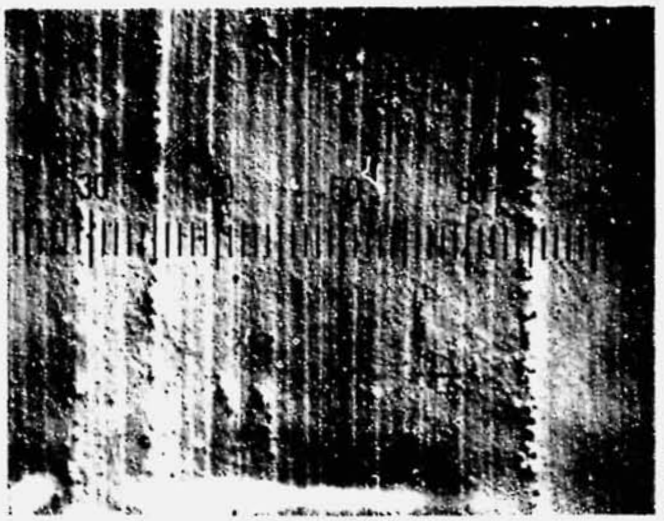

Figure 26 B-swirl precipitate on major striation for a <100> crystal (50 x, each division = 22.2 μm).

Table 4 - Minor Striation Periodicity

Crystal	Orientation	Growth Rate mm/min.	Rotation Rate rpm	Minor Striation μm spacing	Periodicity seconds
007	<111>	1.77	15.5	22.8	.77
		2.47	15.5	34.2	.83
		2.74	15.5	22.8	.50
		2.74	15.5	28.5	.62
		3.0	15.5	11.4	.23
		4.0	15.5	34.2	.51
004	<111>	1.54	6	91	3.5
005	<111>	3.2	15.6	22.8	.43
				91	1.7
		4.6	15.6	34	.44
004	<111>	2.29	6	28	.8
		2.5	22	34	.8
				23	.53
		1.76	22	23	.77
		1.76	30	28	.97
003	<111>	3.83	15	33	.52
				55	.86
001	<100>	2.66	6	22	.5
				44	1.0
				60	1.5

periodicity under various growth parameters. There is no significant trend of the time periodicity with growth speed, rotation rate or orientation. This would indicate that this is a fluctuation in the melt which is not relative to the interface shape. Note that the minor striations show up as faint lines and some could be missed being seen. The Ga doping, planned in the future, should alleviate this possibility and make more precise determinations possible.

III. IMPROVED COIL STUDIES

The source of the major resistivity inhomogeniety in zoned silicon crystals is the slot in the r.f. coil. The slot prevents shorting of the coil and allows current to flow around the coil, as it is an integral part of the r.f. transformer circuit. The slot is an area where the current is concentrated, thus providing a hot spot for heating of the silicon; the part of the coil opposite of the slot is the cold spot. The silicon crystal-melt interface suddenly loses heat as it travels near the cold spot and the melt freezes faster. This incorporates more dopant (and other impurities), providing for a resistivity minimum. When the crystal is cut axially (along its length), this shows up as a resistivity minimum line- or striation.

Minimizing the resistivity variation at the striation could be accomplished by minimizing the thermal fluctuation, which is done by maximizing the r.f. flux uniformity around the coil.

A. Shorted Ring Coil

One concept for eliminating the coil slot is for the slotted coil to induce current into a secondary shorted ring. This would prevent shorting the transformer circuit. Two coil arrangements were selected. Figure 27 shows the drawing for a secondary, shorted work coil which is beneath the slotted coil. The ground connection is made by the cooling water supply tubing. An air gap of 1.25 mm separated the surfaces of the two coils.

The second coil design has the shorted secondary inside the slotted coil, in a co-planar arrangement, as shown in Figure 28 . The gap between coils was slightly eccentric, with a maximum air gap of 1.27 mm, adjacent to the slot in the primary coil. The secondary is grounded to the primary 180° from the slot by silver brazing, with the secondary coil cooling water tubing making the ground connection.

The shape characteristics of the secondary coils was similiar to slot coil designs:

Center hole diameter	= 25 mm
Center edge radius	= 1 mm
Top face slope	= 11 degrees
Bottom face slope	= 7 degrees

Figure 29 shows the bottom views of both coils.

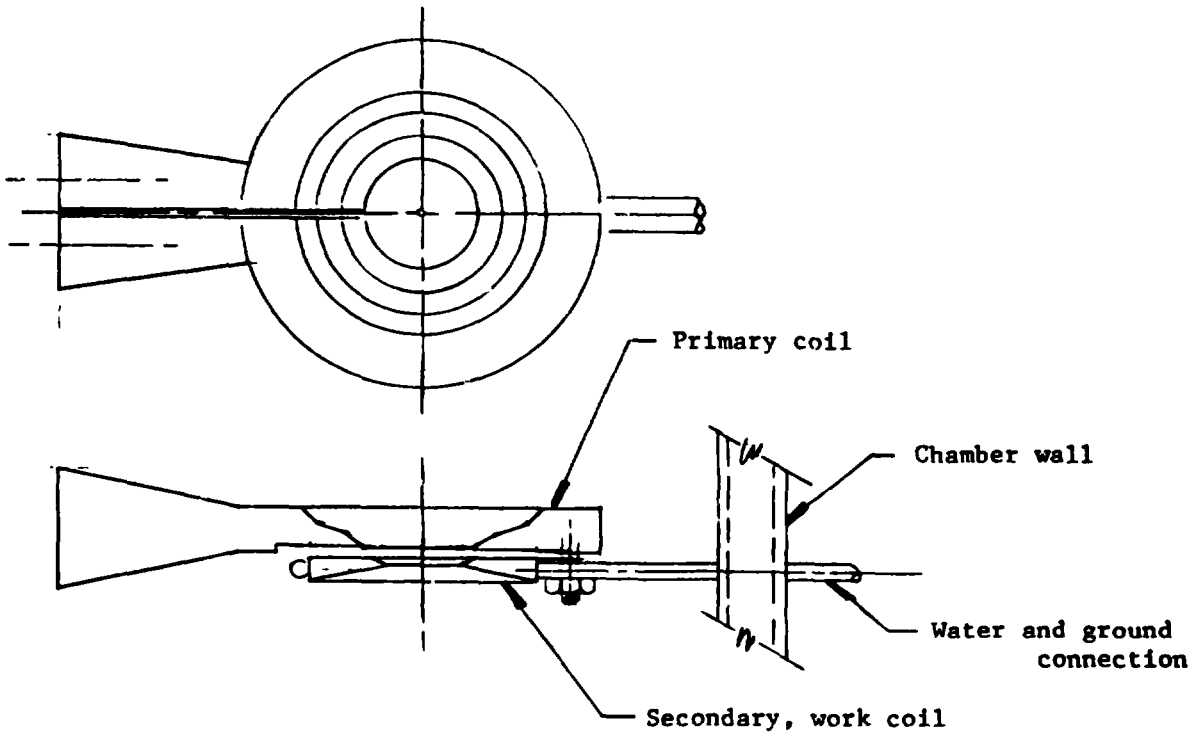

Figure 27

WESTECH SYSTEMS, INC.

SCALE:	APPROVED BY:	DRAWN BY J.M.E.
DATE: 5-20-82		REVISED

AXIALLY DISPLACED CONCENTRIC ARRANGEMENT

DRAWING NUMBER 870-57038

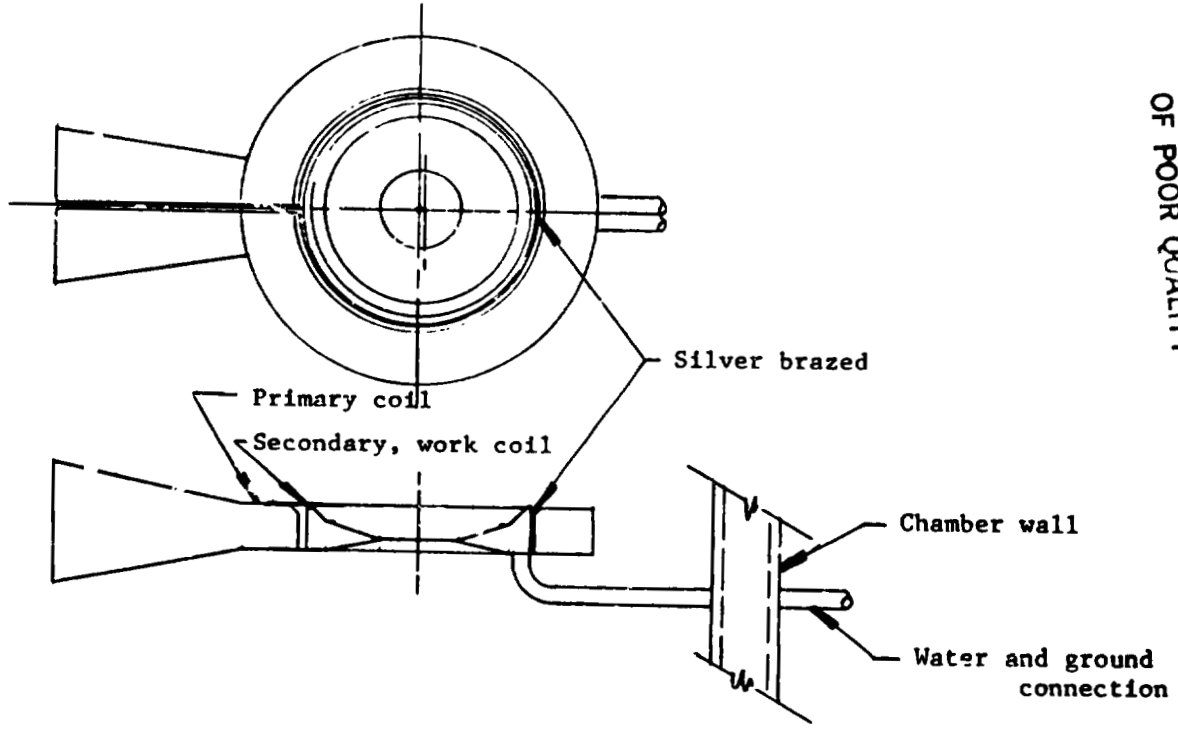

Figure 28

WESTECH SYSTEMS, INC.

SCALE:		APPROVED BY:	DRAWN BY J.M.R.
DATE: 5-20-82			REVISED

CO-PLANAR ARRANGEMENT

DRAWING NUMBER
870-57039

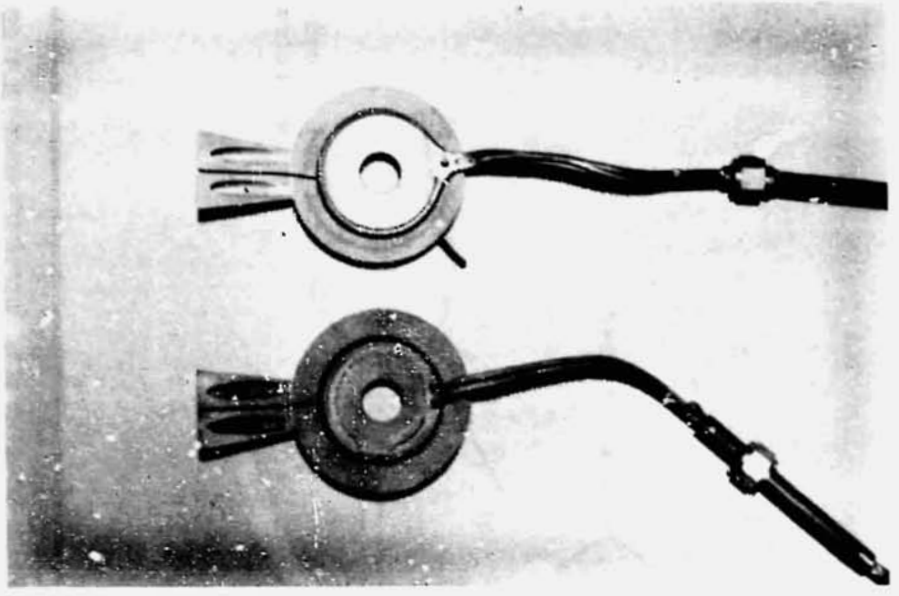

Figure 29 - R.F. Zoning coils with shorted secondary rings. Top: Axially displaced ring. Bottom: Coplanar ring inside slotted coil.

The primary purpose of the experiment was to determine if sufficient R.F. current could be induced in the work coil to provide the electro-magnetic energy required for float zone refining. If this were found to be true, then a second series of experiments would be conducted. These experiments would involve the growth of several crystals with the new method, and comparing their structure to crystals grown with the slotted coil method. Analysis would focus on locating perturbations that could be attributed to the nonuniform field of the slotted coil and their absence in those crystals grown with the new method.

The initial part of the experiments, that of determining the coupling of energy to the work, was conducted with a carbon pre-heater as a load. This provided fast results, since the carbon couples readily to the field. First, the primary only of each new coil was installed. Measurements of plate current and voltage were made with the load well away from the coil, then repeated with the load placed well into the center of the coil. As can be seen from the results shown in Table 5 , a noticeable increase in plate current occurs when the load is coupled. This was true for both primary types and is typical for the slotted coil arrangement when zoning.

Tests of the primary of the arrangement shown in Figure 27 resulted in the load being brought to red heat at a plate voltage of 4 KV and current of 1.6 A with the load spaced about 6 mm from the coil surface.

The primary of the co-planar coil (Figure 28) also brought the load to red heat. The greater distance between coil and load due to the large hole required a plate voltage of 6 KV with subsequent current of 2.4 A.

The primary (shorted) coils were next assembled to their respective secondaries and the previous tests were conducted again. The results this time were markedly different. Introduction of the load into the field had no discernable effect on plate current. Most disappointing, however, was the inability to induce sufficient energy in the load to bring it to red heat.

Neither shorted coil method transferred sufficient energy from the secondary to bring a carbon load to a red heat, with similar lack of heating being expected for silicon.

TABLE 5

Plate voltage and current measurements of the R.F. Power Supply

	Plate Voltage	Current	Load to coil spacing
A. Concentric, axially displaced secondary.			
Primary Only	4 KV	1.18A	No load
	4 KV	1.6 A	6 mm
	4 KV	1.9 A	1.25 mm
Secondary Installed	4 KV	1.2 A	Load had no effect
	7 KV	2.45A	Load had no effect
B. Co-Planar primary and secondary.			
Primary Only	4 KV	1.3 A	No Load
	4 KV	1.4 A	Load up in ring
	6 KV	2.4 A	Load up in ring
Secondary Installed	4 KV	1.45A	No load
	4 KV	1.50A	Load well into center hole
	7 KV	2.9 A	No load
	7 KV	2.9 A	Load well into center hole

B. R.F. Coil Slice Heating

This experiment was designed to provide a visual display of the r.f. energy field that is radiated from the center of the work coil. A silicon wafer was suspended above the work coil and spaced approximately 3.2 mm from the top surface. Application of r.f. power will allow the wafer to be brought to red heat without melting. The shape of the pattern of the red zone should then conform to the shape and intensity of the r.f. field. Irregularities in the shape or width of the red zone would indicate associated irregularities in the shape and intensity of the r.f. field. This should be particularly noticeable in the region around the slot; a "hot spot" here should noticeably alter the shape of the red zone.

To keep the wafer parallel to the coil and to control the gap, the wafer was suspended from the upper work shaft. The upper translation motion control was used to position the wafer with respect to the coil. The wafer was suspended below the work shaft by 3 lengths of copper wire formed to an "L" shape. The wires were inserted in the holes in the work shaft that normally hold the tantalum feed rod chuck fingers. They were then adjusted to ensure the correct positioning of the wafer and secured by set screws (Figures 30 & 31).

Placement of the wafer in a position that was concentric with the coil was not possible. The stud that is utilized to provide an attachment for the center-tap ground connection caused the wafer to be positioned about 6 mm off center, but still in a parallel plane.

The experiment was conducted in three phases:

1. Position the wafer.

2. Pre-heat the wafer, using a typical carbon preheater.

3. After the wafer is brought to red heat, re-position it and vary R.F. heating power to observe the shape and size of the red zone.

Initially, the wafer was positioned about 3.2 mm above the work coil, while the carbon pre-heater was positioned below the coil and about 1.3 cm below the wafer. The R.F. Power Supply was adjusted to a quite low level in comparison to that normally used for float zoning; typically, the pre-heater is at white heat, but in this case, it was heated to a red glow. This was necessary to prevent the wafer from taking heat in a precipitous manner. Under that condition the wafer will literally explode when it transgresses the negative resistance slope.

The first indication that the wafer has been heated past its' critical temperature and is in the negative resistance region is the appearance of a band of silicon that is at red heat. This band is about twice the diameter of the hole in the work

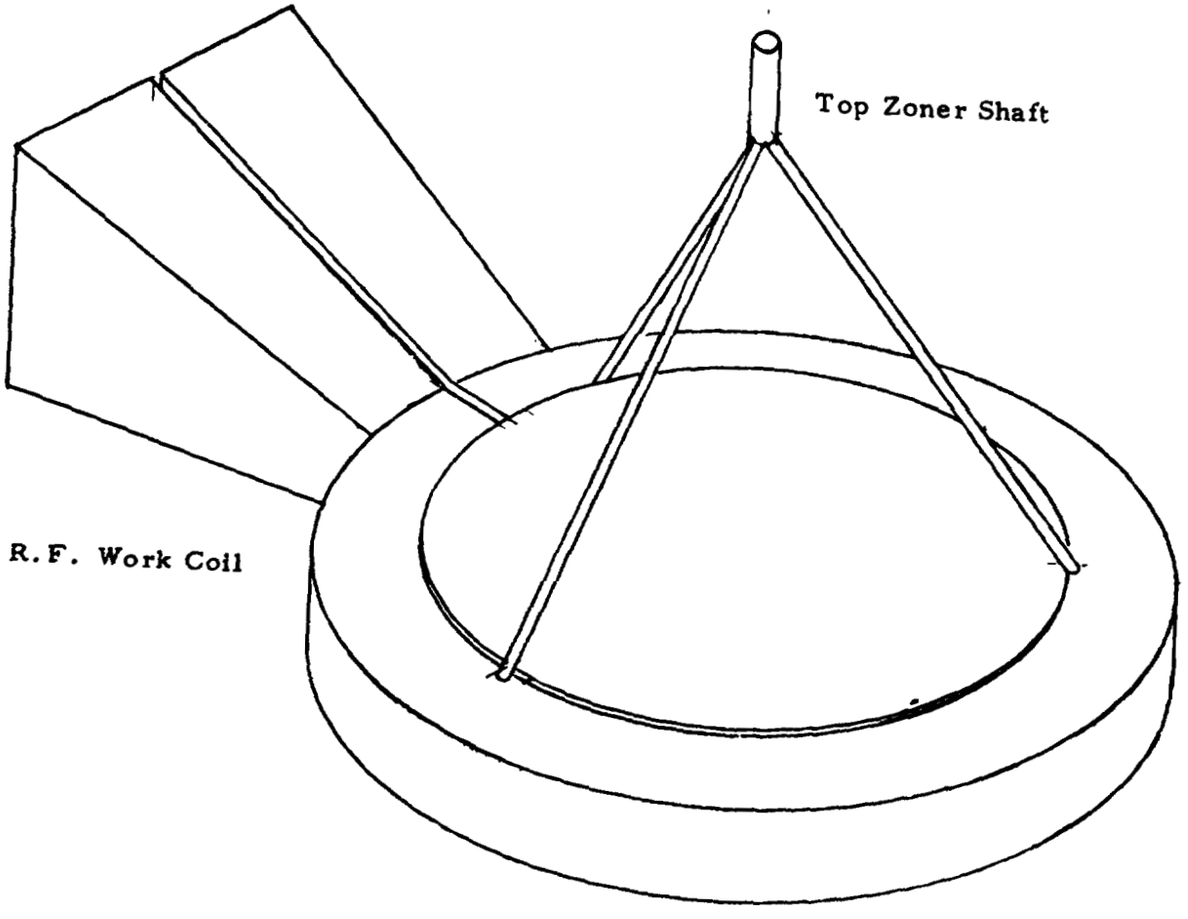

Figure 30

WESTECH SYSTEMS, INC.

SCALE:		APPROVED BY:	DRAWN BY J.M.R.
DATE: 1-6-82			REVISED

WAFER HOLDING FIXTURE

DRAWING NUMBER
870-57050

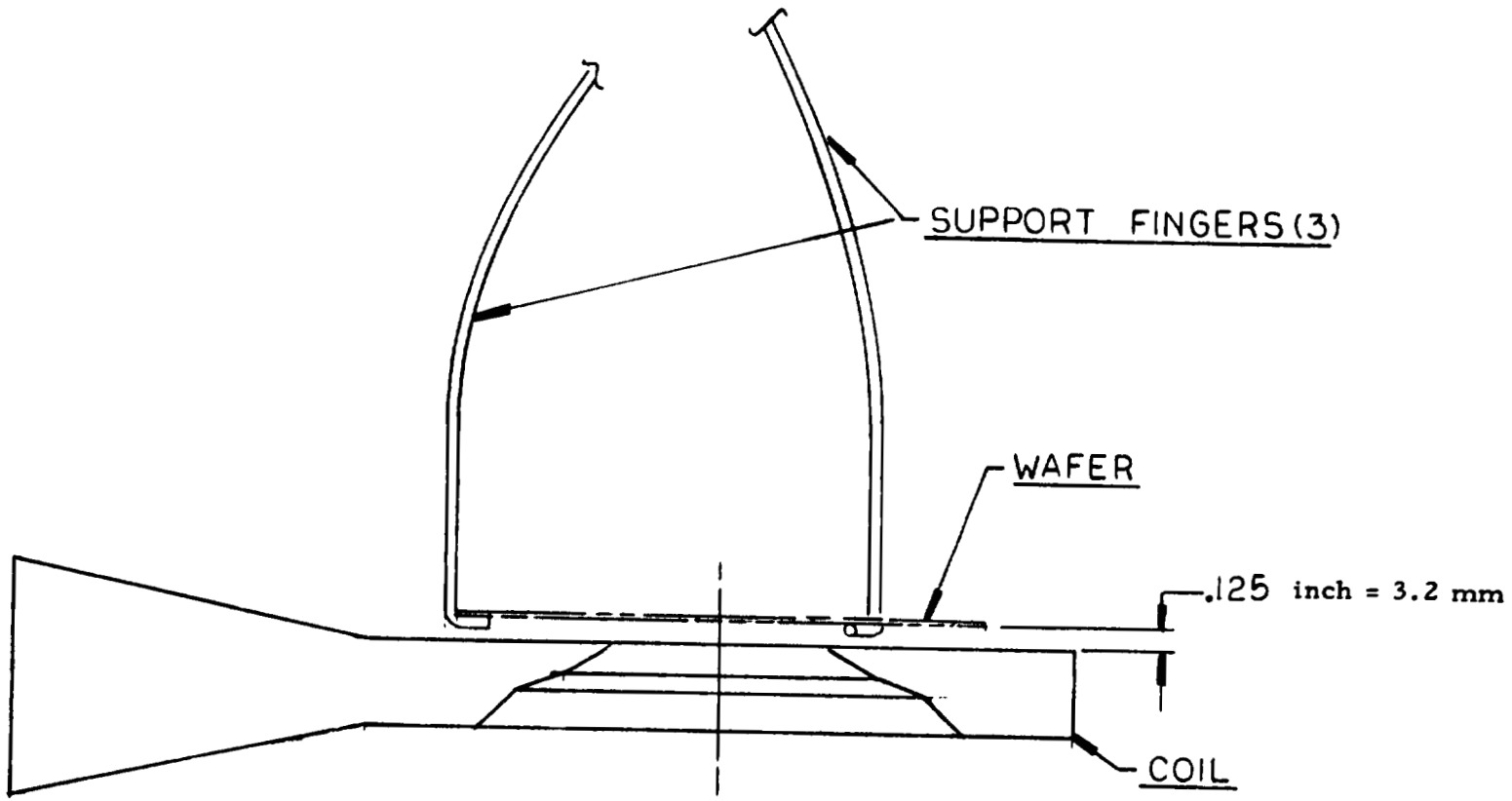

Figure 31

WESTECH SYSTEMS, INC.

SCALE:	APPROVED BY:	DRAWN BY J.M.R.
DATE: 7-6-82		REVISED

COIL—WAFER HOLDING FIXTURE

DRAWING NUMBER
870-57051

coil (4.6 cm) and is about 3 to 4 mm wide. The wafer was then lowered until it was at it's closest proximity to the work coil, a distance of about 2 mm. A slight unsymetrical positioning of the wafer support wires caused the wafer to tilt on levitation. This caused a portion of the wafer to actually melt.

The shape of the red zone was not as originally expected. The hottest portion of the wafer occurred 180° away from the work coil slot. This is possibly explained by noting that the non-concentric placement of the wafer caused less mass at this point, with attending lesser ability to dissipate the heat.

The ring, which is heated most, is the portion of the wafer where the resistivity is reduced the most, which is where the maximum electro-magnetic field is located. Thus, the current is further concentrated in this annular region until melting occurs. (see Figure 32)

C. Proposed Studies

One attempt was made at reducing the current concentration at the coil slot. Figure 33 shows the drawing of a coil with the bottom of the slot, which is closest to the growing crystal, opened wider by machining. Figure 34 shows the opened slot in the coil. A crystal was zoned with this coil. Striation etching indicates there are still regularly spaced rotational meltback striations. Whether the magnitude of resistivity changes is improved would require spreading resistance on an intentionally doped crystal, such as planned for the follow-on program. Additional work will be done on coil slot configuration in the follow-on program.

The experiment on heating a slice indicates that this method of observing the r.f. field may be a promising one to use on analyzing the r.f. field shape. Since the annular ring that melted was much larger diameter than the coil central hole, it also points out that we do not know the shape of the r.f. field above (or below) the coil. This points to a need of analytically understanding the r.f. field. A small study to start this work will be started in the follow-on effort.

An additional transformer-radiator design is scheduled to be built and tried in the next program.

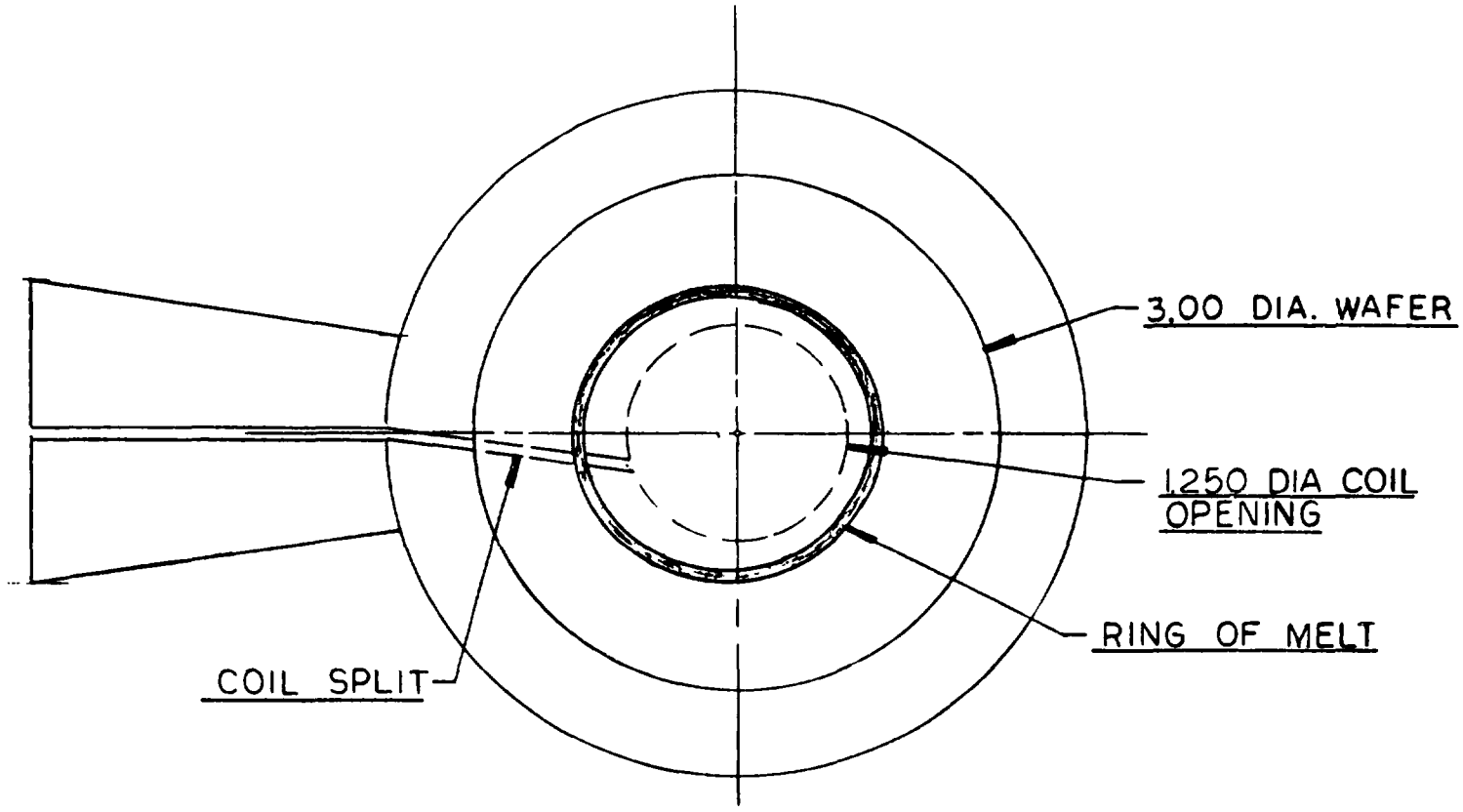

Figure 32

WESTECH SYSTEMS, INC.

SCALE:		APPROVED BY:	DRAWN BY J.H.R.
DATE: 7-6-82			REVISED

WAFER MELT PATTERN

DRAWING NUMBER 870-57052

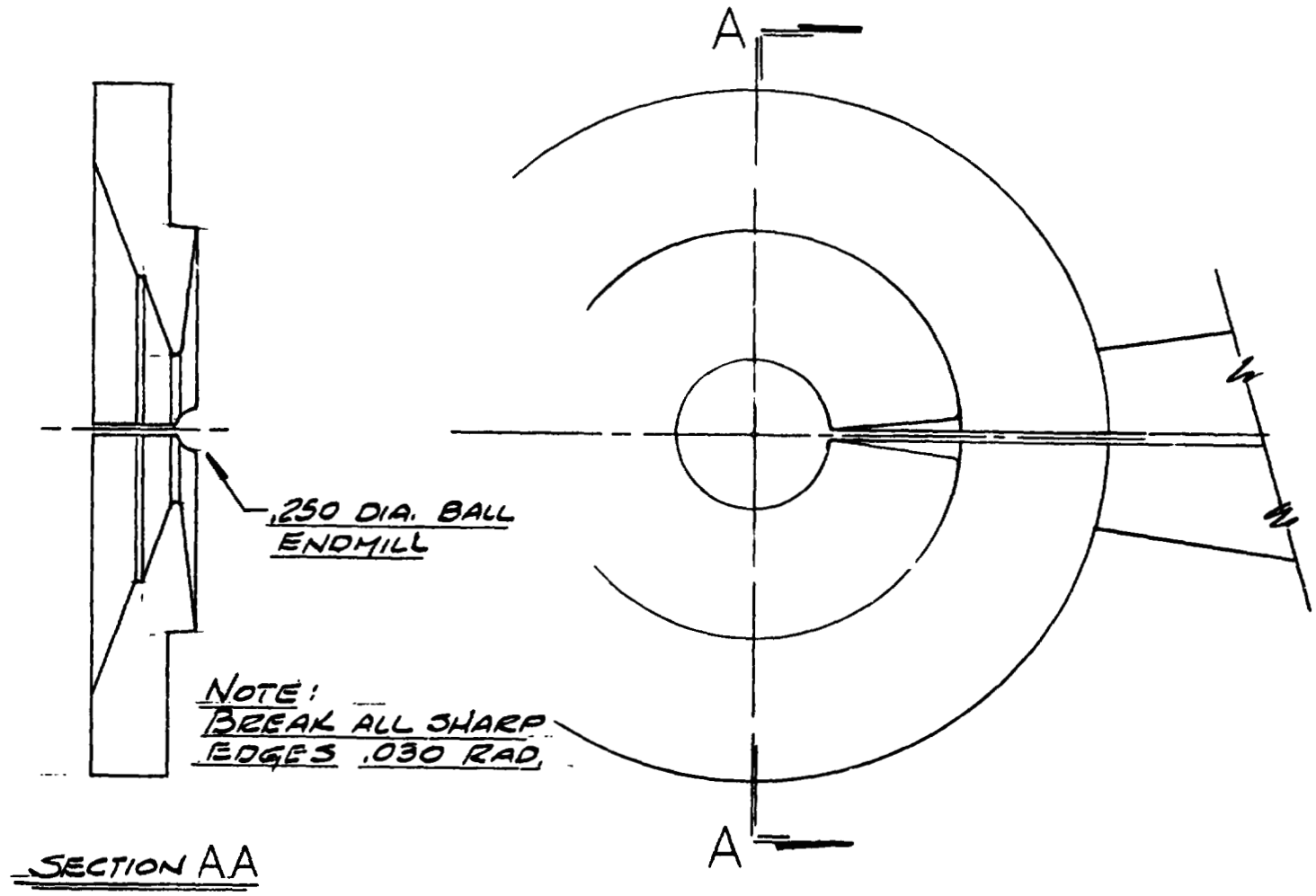

Figure 33

WESTECH SYSTEMS, INC.

SCALE: FULL	APPROVED BY:	DRAWN BY J.MR
DATE: 5-19-82		REVISED

Coil Modification

DRAWING NUMBER 870-57040

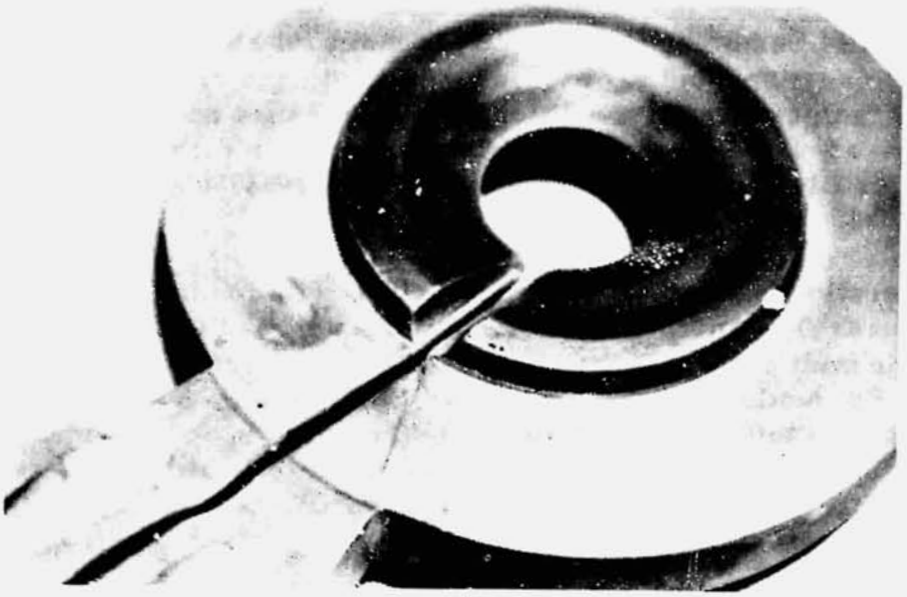

Figure 34 - R.F. Zoning coil with larger slot.

IV. CONCEPTS FOR PRECURSORY FLIGHT EXPERIMENTS

The purpose of this study is to identify meaningful experiments that will provide answers to questions on the differences in float zone crystal growth as one goes from g = 1 to microgravity conditions. These issues need to be addressed in order to justify a major space experiment, with dedicated equipment. The latter, if justified, would be scheduled for the late 1880's, following full definition in 1985.

The key question is whether Marangoni flows will dominate the silicon melt heat and mass flow characteristics, in the absence of bouyancy convection. If it does, the melt could still be turbulent and the interface shape could be quite concave. But neither of these are predictable with the knowledge we now have. By reducing the temperature gradient on the surface, it is conceivable that the flow could be quiescent, that transients in the flow would be absent and that the shape of the growth interface could be controlled. The key to modeling the role of Marangoni flow will be the $\frac{d\sigma}{dt}$ values now being determined by S. Hardy at the National Bureau of Standards. The key to minimizing ΔT might be the Thin Rod Zoning in a modified ADSF furnace discussed below.

A. Slice Zoning Experiments

J. Verhoeven suggested a slice experiment at the 1981 Float Zone Workshop[6] to look at the Marangoni flow on earth and in microgravity. It consists of melting a circular molten zone in a silicon slice and refreezing in a controlled manner. The large surface-to-volume ratio should make the Marangoni flow dominant. It now has to be determined whether there is appreciable bouyancy flow at g = 1 to make a difference in melt flow characteristics between g = 1 and g = 0. If there is not, then ground based experiments will be able to define the Marangoni flow and its behavior by changing grow rates, temperature distribution and the effect of surface agents.

An initial slice heating configuration was set up by J. Zwiener of NASA's Marshall Space Flight Center/Space Sciences Lab, with guidance from E.L. Kern. Anelliptical spot heater is used to heat a silicon slice inside a vacuum chamber by using a quartz window (see Figure 35). A 750 w. heater is capable of supplying 105 watts, or as much as used by Surek[7] to melt a 1 cm diameter in a 0.5 mm thick silicon slice. The heater did melt part of the silicon slice in this experimental setup.

Since the power effeciency is low for the above system, an electron beam heating apparatus is being used to melt silicon slices by I. Dalins of MSFC/SSL. The center of slices have been melted and the characteristic shape of the refrozen crystal, as found by Surek, results. This method does raise questions about possible large ΔT's, but future defocusing of the beam could minimize that.

ORIGINAL PAGE
BLACK AND WHITE PHOTOGRAPH

Figure 35
Elliptical Spot Heater for Silicon Slice

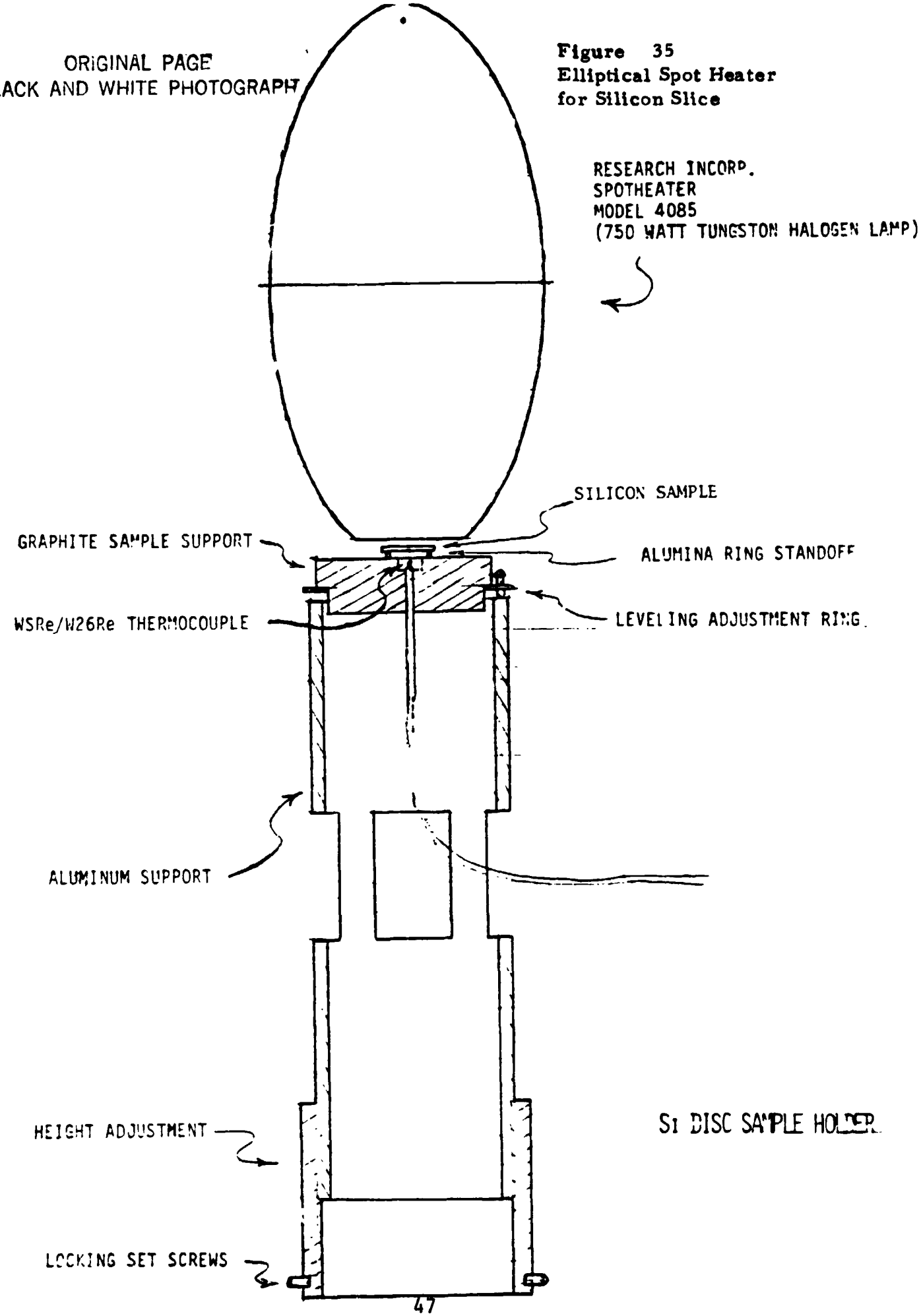

Electromagnetic pressure on the melt from the coupling of the electron beam with a lateral flow of electron current on the surface is also a consideration.

Gallium doped slices will be prepared on the follow-on effort, so that the flow can be characterized by striation etching and/or spreading resistance. The resistivity profile will yield k_{eff}. If flows are similar to 1" diameter float zone growth, k_{eff} should be the same. If the instantaneous growth rate is slower, then k_{eff} will be lower . Oscillatory flows in the melt will give rise to striations, similar to those seen in section II D above.

The effect of surface agents, such as SiO_2 or Si_3N_4, should be to slow surface flows, as long as the melt is not saturated to the point of causing growth to be polycrystalline. The effect should be observed by the above methods.

Analysis of this ground based work will be used to characterize the flows as a function of conditions and to propose a flight experiment if it is needed.

B. Thin Rod Zoning

Power is limited for zoning silicon crystals on early space shuttle flights. The diameters of interest for making devices (50-100 mm or 2 to 4 inches) will take from 5 (very optimistic) to 25 kw power (ref. 6 pages 83-106, 204). Power will be available for testing concepts at 5-7 mm (200-400 watts) (see Table 6 for details, based upon an initial determination by Clayton[8]), on the MEA-B carrier.

Several things can be learned from zoning smaller diameter crystals of silicon:

1) flattening of the growth interface due to lack of bouyancy convection,

2) Effect of longer pseudo-diffusion boundary layers,

3) Effect of the gaseous zoning atmosphere not having convection,

4) Effects of Marangoni convection.

Some things will not be learned. The shape of the growth interface at small diameters is much different than at large diameters (section II-D above). While the convex growth interface should give superior crystallography (section II-D above), it indicates that scaling the diameter up will involve substantial interface shape change, which will then affect lateral solutal flows.

The method of heating needs to be optimized both to minimize power inefficencies and to maximize uniformities in temperature and crystal properties. The methods to be compared are:

1) Hot wall furnace,

2) Elliptically focused light from hot filaments,

Table 6 Flight Experiment Plan for M.E.A. Zoning of Silicon

M.E.A. Flt. #	Sample #	Composition	Max. Power Watts	Zoning Speed mm/min.	Length Regrown Crystal mm	Zoning Time min.	Total Time hrs.	Gas Ambient	Total Power Watt-hr.	TOTAL FLIGHT POWER kw-hr.
1 (1984)	1	Ge:Ga	100	2	20	1.0	.42	vac.	42	
	2	Si:Ga	200	2	20	10	.42	vac.	83	
	3	$Si_{30}Ge_{70}$:Ga	100	$2x10^{-2}$	2	100	2.0	vac.*	200	.325
2 (1985)	1	Ge: Ga	100	1&2	40	30	1	vac.	100	
	2	Si: Ga	200	1, 2, 5	75	42	1	vac.	200	
	3	$Si_{30}Ge_{70}$:Ga	100	$2x10^{-2}$	20	1000	17.2	vac.	1720	7.5
	4	$Si_{50}Ge_{50}$:Ga	150	$2x10^{-2}$	20	1000	17.2	vac.	2580	
	5	$Si_{70}Ge_{30}$:Ga	170	$2x10^{-2}$	20	1000	17.2	vac.	2670	
	6	Si:In($3x10^{17}$)	200	1, 2, 3	75	45	1.1	Ar	220	
3 (1986)	1	Si:Ga	200	1, 2, 5	75	42	1	vac.	200	
	2	$Si_{50}Ge_{50}$:Ga	150	$2x10^{-2}$	50	2500	42.2	vac.	6325	
	3	$Si_{60}Ge_{40}$:Ga	155	$2x10^{-2}$	50	2500	42.2	vac.	6540	14.1
	4	Si:In($4x10^{17}$)	200	0, 5, 1	50	75	1.7	Ar	340	
	5	Si:TL	200	0, 5, 1	50	75	1.7	Ar-2atm	340	
	6	Si:TL &Sn	200	0, 5, 1	50	75	1.7	Ar-2atm	340	
4 (1986)	1	Si:Ga(7mmϕ)	400	0, 5, 1, 3	100	103	2	vac.	800	
	2	$Si_{20}Ge_{80}$:Ga	100	$2x10^{-2}$	50	2500	42.2	vac.	4220	
	3	$Si_{40}Ge_{60}$:Ga	125	$2x10^{-2}$	50	2500	42.2	vac.	5275	18.3
	4	$Si_{80}Ge_{20}$:Ga	180	$2x10^{-2}$	50	2500	42.2	vac.	7600	
	5	Si:S	200	1, 2	50	37	1	Ar-2atm	200	
	6	Si:Se	200	1, 2	50	37	1	Ar-2atm	200	

*vac. = 10^{-6} torr, AR = 1 atm. Argon (unless stated)

3) R.F.

4) Electron beam.

The hot wall furnace (like the ADSF (automated direction solidification furnace, platinum wire heater) has never been tried for zoning. It has the advantages of requiring low voltage, of flexibility in profiling the temperature distribution and of the prospect of good power effeciency.

The elliptically focused heaters have been shown to be suitable for zoning silicon[9,10]. The heaters that focus into one or two (or more) sides of a cylinder will create large ΔT's, which will drive the Marangoni convections (as much as 25-50° C). The monoellipse furnace which heats 360° around the cylinder is much preferred. The efforts of Eyer and Nitsche should be followed for progress on this technique. The heating elements which are concentric around the cylinder and focused in a toroidal-ellipsoidal fashion will be of lower effeciency since more of the light has to bounce one or multiple times off the (imperfect) reflecting walls. (This is the Semtech furnace design[8].)

R.F. heating presently lacks good power conversion effeciency and uniformity of power going into the crystal (due to a very concentrated induced heating from a very thin coil and the coil slot). It does have the advantage that it is the standard method for zoning silicon and there is a lot of experience in this area. Improvements are planned and the reduction of these problems will be monitored. Electron beam methods will be at a disadvantage from the high voltage necessary (and power ineffeciency to get there) and low power effeciency in creating the electron beam, which will be made even lower by zoning in a gas atmosphere, where the beam has to be extracted from a vacuum-chamber filament area and then interact with the gas.

Heat and mass flows in microgravity will be different than at g = 1 . We do not know whether the advantages of zoning dislocation free crystals in gas (argon, slightly above atmospheric pressure) at g = 1 will extend to microgravity growth.

The hot wall furnace now looks the most promising for initial development for zoning silicon in space. Extensive ground based development will be needed to gain the experience with this method to successfully zone at small diameters. Since there is no r.f. coil slot caused rotational meltback striations to demarcate the growth interface, it will be necessary to do so by a Peltier pulse which will either quickly freeze or quickly melt material at the interface. A current pulse of 6 amperes (15 amps/cm^2 at 7 mm diameter) with a pulse width of 0.01 - 0.1 seconds and spacing of 0.1 to 1.0 seconds should be adequate for silicon at this diameter.

A conceptual sketch for a hot-wall (modified ADSF) furnace is shown in Figure 36. The heater designs and passive hot walls (reflectors and insulators) can be determined emperically or with the aid of analytical programs, such as proposed by L. Foster (ref. 6 p. 188-199). Figure 37 shows one conceptual layout of the hardware in a M.E.A. cannister. It is also conceivable that the experiments could be done in a mid-deck apparatus, depending on the power available. The length of zoning and flexibility is expected to be limited there by a height limitation.

Figure 36 CROSS SECTION OF FURNACE

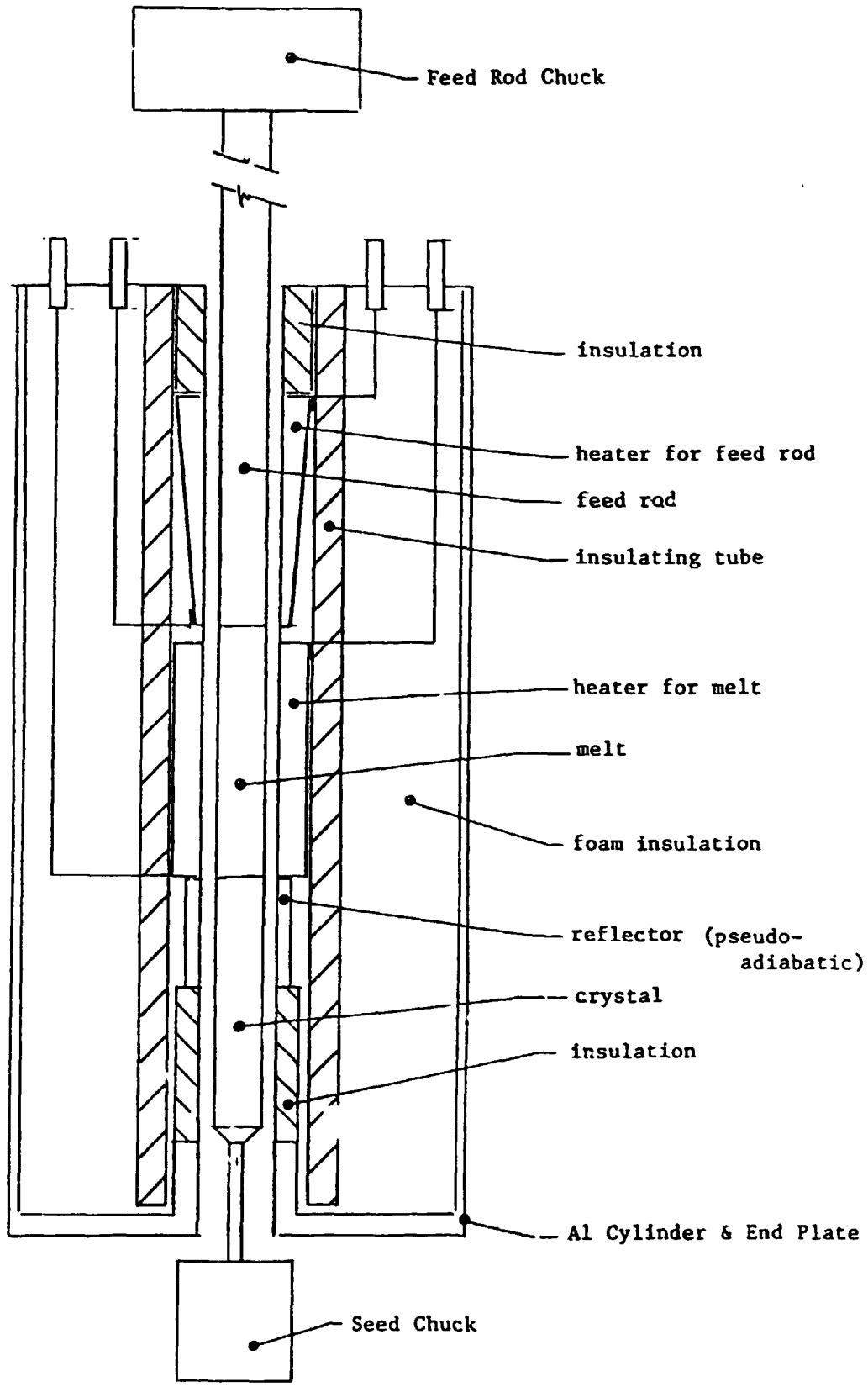

Figure 37 Silicon Zoning M.E.A. Cannister

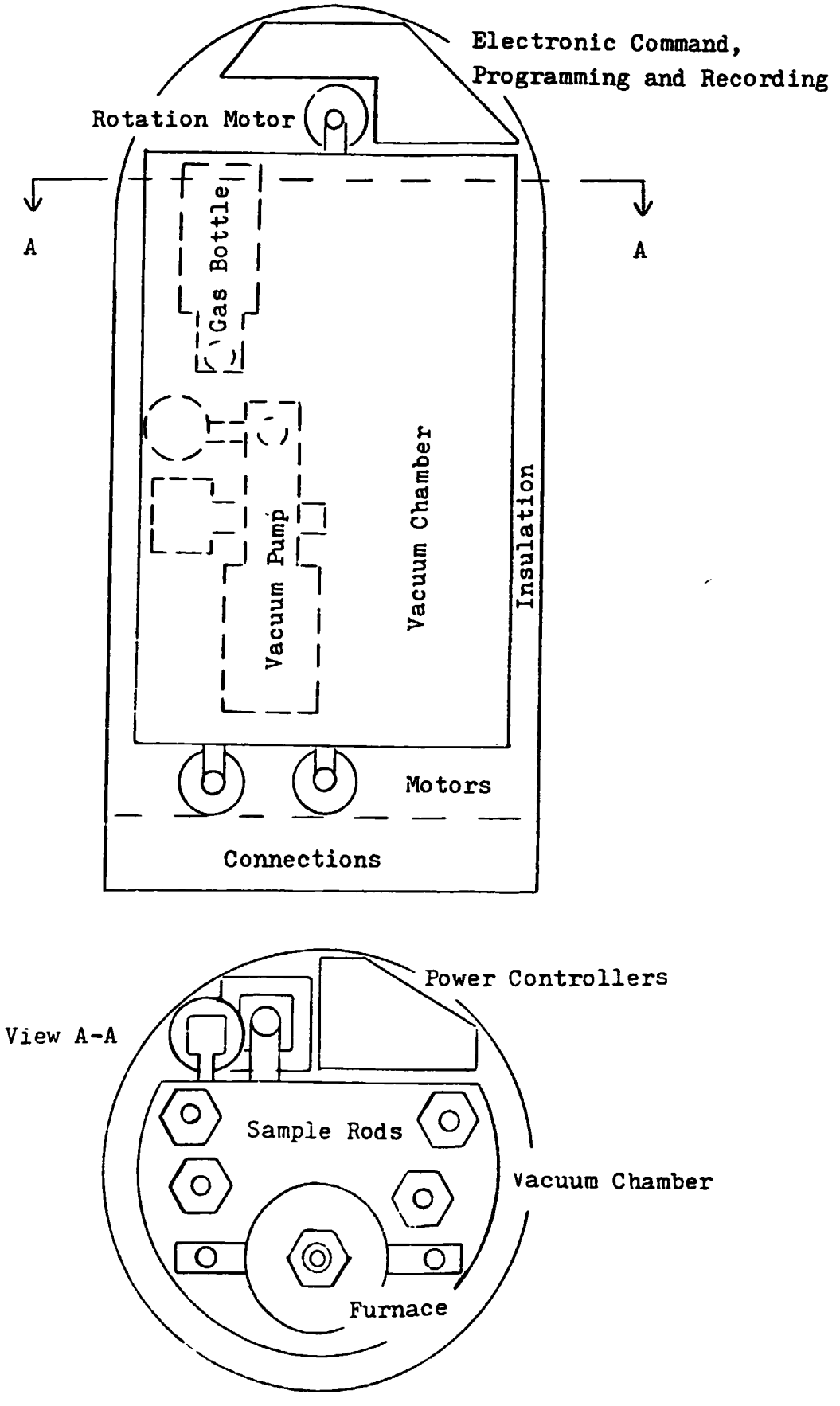

The recommended vehicle for the Thin Rod Zoning is the M.E.A. cannister. A height of 91 cm (36 inches) would be needed to zone 15 cm long crystals (6 inches) in an 18 cm long hot wall furnace. This provides the necessary flexibility to neck the seed transition and to rotate the solid rods. Proposed zoning times and powers are shown in Table6 . A flight unit could be ready to fly in late 1984, needing one year to do the preliminary ground experimentation leading to design of experiments and definition of flight hardware. If done in an expeditions manner, the flight hardware, further ground experimentation and ground based flight hardware checkout could be done in another year.

C. Silicon : Germanium Crystals

Si:Ge alloys have intermediate properties (bandgap, melting point, lattice spacing & density) between silicon and germanium. The band gap (0.65 to 1.09 eV) makes it a very good intrinsic light detector in the 1.0 to 2.0 μm infrared range. New detectors are needed for the 1.3 - 1.5 μm range for fiber optic communication detectors. III-V quaternaries (Ga, Al, As,P) are now being developed. For these, new microcircuit fabrication technologies need to be developed, expecially in production. If silicon technology could be used, as is a possibility with Si : Ge, then any silicon production line would already have the necessary technology and new facilities wouldnot be required. This could save industry over $100 million in development and hardware costs. Si :Ge chips could be bonded to silicon chips for signal processing. The key to this possibility is growing the Si : Ge alloy of the desired composition and testing its properties for device fabrication. This includes the necessity to grow a good thermal SiO_2 layer for masking. This should be shown as early as possible in a developmental program.

$Si_x : Ge_{1-x}$ alloys cannot be grown at g = 1 where $10 \leq x \leq 90\%$. In the intermediate region, the Ge segregates to the bottom of a horizontal boat and constant composition cannot be maintained. If zoned in a vertical position at g = 1, zoning up (normal) would rapidly concentrate Ge at the growth interface, depleting the lighter Si atoms. In down zoning, the Ge would be depleted from the growth interface (now at the top of the zone), also leading to compositional inhomogeneity. Furthermore, the growth rate for mid-gap material needs to be $\leq 2 \times 10^{-2}$ mm/min.[11] This slow instantaneous growth rate is also difficult to maintain at g = 1 due to bouyancy convection instabilities and should be easier in microgravity conditions.

It is compatible to consider zoning Si : Ge crystals in the same apparatus as silicon, including the M.E.A. flight possiblities. Initial accomplishment of the lack of Ge segregation could be shown by horizontal zoning of the slice experiment nature (section A above) in microgravity.

D. Flight Possibilities

The possibilities for experimenting in microgravity are:

Get-away special cannister (GAS-CAN)
Mid-deck
Materials Experimental Apparatus (M.E.A.)
Shuttle pallet-dedicated
Space-lab

Space-lab does not have sufficient power (600 watts total) for any appreciable diameter or length. A dedicated pallet in the shuttle bay is expensive and should be used for scaled up development after the feasibility is shown. O-gravity times in the KC - 135 (1/2 minute) or sounding rockets (several minutes) are too short for any characterization of the melt conditions and their variation. Initial power limitations and possible diameters are:

Carrier Mode	Available Power	Silicon Diameter
GAS-CAN	3.5 kw-hr.	slices
MEA - A	0.5 kw-hr.	5 mm
MEA - B	2.6 kw/hr.	5 - 25 mm
Shuttle Pallet (or possibly MEA-C)	8 kw/hr.	50 mm

It is recommended that MEA-B, which can easily handle the power needs shown in Table 6, be considered for initial Thin-Rod Zoning experiments.

REFERENCES

1. W. Keller & A. Muhlbauer, "Floating-Zone Silicon" Marcel Dekker, New York (1981) p. 118

2. E.L. Kern, Paper A-1, Conf. on Preparation and Properties of Electronic Materials, A.I.M.E., Boston, Mass. (Sept. 9, 1974)

3. M. Kamper, JECS 117 no. 2 p. 261-2 (Feb. 1970)
   K.R. Mayer, JECS 120 no. 12 p. 1780-82 (Dec. 1973)

4. E. Bauser and G.A. Rozgonyi, JECS 129 no. 8 p. 1782-85 (Aug. 1982)

5. A.J.R. deKock, P.J. Roksnoer and P.G.T. Boonen, J. Crystal Growth 22 311 (1974)

6. J. Verhoeven, p. 147 NASA Conf. Publication 2226 "Float Zone Workshop" Sept., 1981 Ed: E.L. Kern & E.K. Cothran

7. T. Surek & B. Chalmers, J. Cryst. Growth 29 (1975)

8. C. Clayton, calculations (private conversation)

9. A. Eyer and R. Nitsche, Proceedings, 3rd European Symposium on Materials Science in Space, Grenoble, France p. 75 (April 24-27, 1979)

10. A. Eyer, H. Leiste, M. Schuhmacher and H. Walcher, "Building and Testing a Monoellipsoid Mirror Heating Facility" (Advanced copy of paper submitted for publication)

11. J. P. Dismukes and L. Ekstrom, Trans. Metallurgical Soc. of A.I.M.E. 233 (Apr. 1965)

☆U.S. GOVERNMENT PRINTING OFFICE: 1982—646-058/91